HHS Public Access

Author manuscript

Cell Host Microbe. Author manuscript; available in PMC 2024 July 12.

Published in final edited form as:

Cell Host Microbe. 2023 July 12; 31(7): 1154–1169.e10. doi:10.1016/j.chom.2023.05.030.

Generation of host-directed and virus-specific antivirals using targeted protein degradation promoted by small molecules and viral RNA mimics

Nan Zhao[1,2,9], **Jessica Sook Yuin Ho**[1,9], **Fanye Meng**[3,9], **Simin Zheng**[1], **Andrew P. Kurland**[1], **Lu Tian**[4], **Martha Rea-Moreno**[5], **Xiangyang Song**[3], **Ji-Seon Seo**[8], **H Ümit Kaniskan**[3], **Aartjan J W te Velthuis**[6], **Domenico Tortorella**[1], **Ya-Wen Chen**[7], **Jeffrey R. Johnson**[1], **Jian Jin**[3,*], **Ivan Marazzi**[1,2,8,10,*]

[1]Department of Microbiology, Icahn School of Medicine at Mount Sinai, New York, NY 10029, USA

[2]Global Health and Emerging Pathogens Institute, Icahn School of Medicine at Mount Sinai, New York, NY, USA

[3]Mount Sinai Center for Therapeutics Discovery, Departments of Pharmacological Sciences and Oncological Sciences, Tisch Cancer Institute, Icahn School of Medicine at Mount Sinai, New York, NY 10029, USA

[4]Department of Otolaryngology, Icahn School of Medicine at Mount Sinai, New York, NY 10029, USA

[5]Department of Otolaryngology, Master of Science in Biomedical Science Program, Icahn School of Medicine at Mount Sinai, New York, NY 10029, USA

[6]Lewis Thomas Laboratory, Department of Molecular Biology, Princeton University, NJ 08544, USA

[7]Department of Otolaryngology, Department of Cell, Developmental and Regenerative Biology, Black Family Stem Cell Institute, Institute for Airway Sciences, Icahn School of Medicine at Mount Sinai, New York, NY 10029, USA

[*] Correspondence: jian.jin@mssm.edu, imarazzi@uci.edu.

AUTHOR CONTRIBUTIONS

I.M. conceived the concept of this whole project. I.M. and J.J. (Jian Jin) co-supervised this study. F.M., X.S., and H.Ü.K. designed and synthesized small-molecule compounds. J.S.H., N.Z., and A.J.W.tV. designed RNA oligonucleotides. N.Z., J.S.H., S.Z. and J.S conducted the biological evaluations and validations of small-molecule compounds and RNA oligonucleotides. A.K. and J.J. (Jeffrey Johnson) performed the proteomics assays and processed the quantitative analysis. L.T., M.R-M., and Y.C. provided human lung organoids. D.T. provided cells and viruses. N.Z., J.H., and I.M. wrote the manuscript.

DECLARATION OF INTERESTS

Mount Sinai School of Medicine has filed patents covering the use of small molecule-based GSPT1 degraders and RNA oligonucleotide-based viral polymerase Destroyers as novel antiviral strategies. J.J. (Jian Jin) is a cofounder and equity shareholder in Cullgen, Inc., a scientific cofounder and scientific advisory board member of Onsero Therapeutics, Inc., a consultant for Cullgen, Inc., EpiCypher, Inc., Accent Therapeutics, Inc, and Tavotek Biotherapeutics, Inc. The Jin laboratory received research funds from Celgene Corporation, Levo Therapeutics, Inc., Cullgen, Inc., and Cullinan Oncology, Inc.

[8]Department of Biological Chemistry, University of California, Irvine, CA 92697, USA

[9]These authors contributed equally

[10]Lead contact

SUMMARY

Targeted protein degradation (TPD), as exemplified by proteolysis-targeting chimera (PROTAC) is an emerging drug discovery platform. PROTAC molecules, which typically contain a target protein ligand linked to an E3 ligase ligand, recruit a target protein to the E3 ligase to induce its ubiquitination and degradation. Here, we applied PROTAC approaches to develop broad-spectrum antivirals targeting key host factors for many viruses and virus-specific antivirals targeting unique viral proteins. For host-directed antivirals, we identified a small molecule degrader, FM-74–103, that elicits selective degradation of human GSPT1, a translation termination factor. FM-74–103 shuts down translation initiation, inhibiting both RNA and DNA viruses. Among virus-specific antivirals, we developed viral RNA oligonucleotide-based bifunctional molecules (Destroyers). As a proof-of-principle, RNA mimics of viral promoter sequences were used as heterobifunctional molecules to recruit and target influenza viral polymerase for degradation. This work highlights the broad utility of TPD to rationally design and develop next generation antivirals.

Graphical Abstract

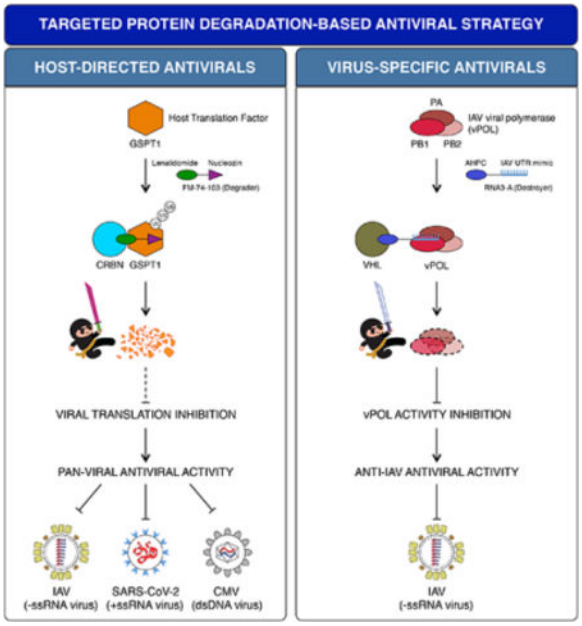

eTOC Blurb

In this study, Zhao, Ho, and Meng et. al. use proteolysis-targeting chimera (PROTAC) modalities to develop antiviral molecules. Broad spectrum antiviral activity can be achieved using conventional small molecule-based degraders targeting host factor GSPT1, while virus-specific antiviral activity can be achieved using viral RNA oligonucleotide-based Destroyers targeting viral polymerase.

INTRODUCTION

Viral infections are major threats to human health and pose immense burdens to global healthcare systems and economies. This has been exemplified by the current coronavirus disease 2019 (COVID-19) pandemic, caused by severe acute respiratory syndrome coronavirus 2 (SARS-CoV-2),[1] as well as by other major epidemics and pandemics throughout history. For example, annual epidemics caused by influenza viruses result in approximate 3 to 5 million cases of severe illness globally while occasional pandemics, such as the 1918 influenza pandemic, can affect mortality rates worldwide.[2] To circumvent crises associated with viral infections, a continued effort for prevention and control of virus infections is needed. The emergence of novel viruses and the appearance of drug-resistant strains among known viruses also urge for the development of novel antiviral therapies.[3]

Targeted protein degradation (TPD) is an upcoming drug discovery strategy that utilizes hetero-bifunctional modalities to eliminate a protein of interest (POI) in human cells by hijacking intracellular proteostasis machinery, such as the ubiquitin-proteasome system (UPS), macroautophagic pathway, and endolysosomal pathway.[4] As a classic representative of TPD, proteolysis-targeting chimera (PROTAC) molecules typically comprise a POI ligand, a linker and an E3 ligase ligand. These heterobifunctional molecules initially recruit the POI in proximity to the E3 ligase, subsequently promote the ubiquitylation of the POI, and eventually induce the degradation of the POI by the proteasome.[5] Since the first PROTAC example was reported in 2001,[6] stunning progress has been made by implementing this type of TPD in the field of cancer research in the last two decades.[7] In the recent years, there has been increased interest in harnessing PROTAC technology in the development of antiviral therapies.[8–15] However, this area of study remains underexplored. In this study, we investigated whether PROTAC modalities can be used to target either host proteins or viral proteins for degradation to further achieve host-directed or virus-specific antiviral effects.

We generated conventional small-molecule PROTAC modalities as host-directed antivirals and assessed their capacity to degrade key host factors controlling the replication of both RNA and DNA viruses in host cells. We also developed a virus-specific antiviral strategy by applying bifunctional molecules in which traditional small molecules were substituted with viral RNA mimics to attract RNA-binding viral proteins with high specificity for viral RNAs and evaluate their antiviral potency.

Below, we provide proof-of-principle that 1) targeted degradation of a host factor can be an effective antiviral approach against many divergent viruses; and 2) viral RNA mimics can be used to develop virus-specific antiviral therapies. We discuss the potential of both strategies to generate antivirals.

RESULTS

103 inhibits IAV replication

To verify if TPD is a feasible paradigm for influenza antiviral drug development, we first selected Nucleozin (Figure 1A) as the small-molecule ligand to make PROTAC molecules. Nucleozin is a potent IAV inhibitor that targets nucleoprotein (NP) and causes

NP aggregation.[16] A library of the conjugates of Nucleozin with phthalimide analogues (Thalidomide/Lenalidomide/Pomalidomide), one most frequently used E3 ligase ligand, was designed and built. Screening of the library by using a recombinant IAV carrying a GFP reporter in the NS segment (NS1-GFP PR8 virus) allowed us to identify a compound, FM-74–103 (hereafter 103) (Figure 1A, see the synthetic details in Supplementary Information), that can greatly inhibit the replication of NS1-GFP PR8 virus[17] in A549 cells without conferring observable cytotoxicity (Figure 1B, Figure S1A). We then used plaque assays to quantify titers of A/Puerto Rico/8/34 (H1N1) (WT PR8) virus grown in A549 cells treated with 103. 103 exhibited comparable inhibitory activity of Nucleozin against WT PR8 replication in A549 cells (Figure 1C) while displaying negligible effects on cell viability (Figure 1C, top, Figure S1A). This is also supported by the reduced levels of NP seen in the infected cell lysates treated with either Nucleozin or 103 (Figure 1C, bottom). We further assessed the dose-responses of Nucleozin and 103 by comparing their anti-IAV potencies in primary human brochial/tracheal epithelial (HBTE) cells. Both compounds exerted anti-WT PR8 potency at similar levels in HBTE cells without affecting cell viability (Figure 1D, left, Figure S1A). Additionally, 103 retained anti-IAV activity against A/Netherlands/602/2009 (H1N1), a Nucleozin-resistant IAV strain expressing NP with a tyrosine at 289 to histidine mutation (Y289H) isolated from human patients (Figure 1D, right, Figure S1B).[16] This observation confirms that 103 activity is independent of, and distinct from, Nucleozin. Accordingly, 103 did not confer its anti-IAV effect through promoting the aggregation of NP as Nucleozin does (Figure S1C).

We then performed quantitative proteomic analysis of the whole cell lysates of DMSO- and 103-treated cells before and after infection. Our analysis indicates that the levels of all the IAV proteins in A549 cells were significantly decreased by treatment of 103 compared to DMSO for 24 hours post infection (Figure 1E, right, 1F, and Supplementary Table 1). Aside from IAV proteins, the host protein that exhibited the strongest downregulation was the translation termination factor GSPT1 (G1 to S phase transition 1) (Figure 1E, 1F, and Supplementary Table 1). It is noteworthy that in uninfected A549 cells, 103 also induces downregulation of GSPT1 within only 4 hours of treatment (Figure 1E, left). We therefore sought to determine if the anti-IAV effect of 103 was indeed a result of NP degradation or GSPT1 degradation.

103 selectively depletes human GSPT1

If the anti-IAV potency of 103 is the result of inducing NP degradation, we would expect that 103 can induce the degradation of “preexistent” NP, in the absence of infection. This was not the case. In A549 cells where NP was expressed via plasmid transfection for 24 hours prior to 103 treatment, no degradation was observed (Figure S2A, left). Instead, when A549 cells were concurrently transfected with NP plasmid and treated with 103 for 24 hours, the NP level was dramatically diminished (Figure S2A, right). This observation suggests that 103 suppresses the transient expression of NP in A549 cells. Additional evidence further indicates that this suppressive effect of 103 is not exclusive to NP. In fact, the expression levels of many other transfected genes from both endogenous and exogenous origins (regardless of their molecular weights and biochemical functions) were all reduced

by the treatment of 103 (Figure S2B). This result suggests that anti-IAV effect of 103 was not likely elicited from the direct degradation of NP.

We next asked if 103-mediated degradation of GSPT1 could contribute to the anti-IAV activity of 103. GSPT1 has been biochemically characterized as a factor that stringently regulates the translation termination in eukaryotes.[18] Since host translation regulation plays a key role in viral replication, we reasoned that 103-induced depletion of GSPT1 in A549 cells can impair the termination stage of the translation of IAV mRNA, resulting in the inhibition of IAV replication in A549 cells. To validate this hypothesis and confirm our initial proteomics analysis (Figure 1E and 1F), we measured the protein levels of GSPT1 in uninfected A549 cells with and without 103 treatment. We found that 103-induced degradation of GSPT1 in A549 cells is time- (Figure 2A) and concentration- (Figure 2B) dependent. The effect of 103 is also reversible, as indicated by washout experiments (Figure 2C). eRF1 (eukaryotic peptide chain release factor 1; encoded by *ETF1*),[18] a factor that interacts with GSPT1 to govern the translation termination in eukaryotes, was also notably destabilized with the depletion of GSPT1 (Figure 2A–2C). 103-driven degradation of GSPT1 was not due to the decreased level of the *GSPT1* mRNA as shown in RT-PCR (Figure S2C). Instead, it was strictly dependent on the abundance of cereblon (CRBN), as evidenced by the attenuation of 103's effect on lowering GSPT1 levels in cells treated with *CRBN* targeting small interference RNA (siRNA) (Figure 2D). Additional factors required to complete 103-promoted GSPT1 depletion include the formation of the ternary complex GSPT1–103-CRBN, active neddylation, and a functional proteasome, as exhibited in competition assay using verified inhibitors against the different steps in ubiquitin-proteasome pathway (Figure 2E). Notably, 103 also induced significant ubiquitylation of GSPT1 in a pull-down assay (Figure 2F), suggesting that 103 acts as a *bona fide* recruiter of GSPT1 to UPS and promotes its degradation.

Although both Nucleozin and Lenalidomide (Figure 1A) moieties in 103 are required for the elimination of GSPT1, the contributions were apparently not equal since co-treatment of Nucleozin conferred a weaker competitive effect (Figure 2E). To further confirm that the Nucleozin moiety is essentially required for 103-dependent destruction of GSPT1, we purified two intermediate compounds in the synthetic route of 103, FM-123–96 and FM-123–142 (hereafter 96 and 142) (Figure 1A, see the synthetic details in Supplementary Information), in which Nucleozin moiety in 103 was removed and linker-Lenalidomide moiety was preserved. When A549 cells were simultaneously transfected with GFP plasmid and treated with 96 or 142 for 24 hours, 96 and 142 did not induce degradation of GSPT1 and inhibit the transient expression of GFP in A549 cells (Figure 2G). This indicates that the moiety of Nucleozin in 103 is indispensable for 103-mediated depletion of GSPT1. In addition, CC-885 (hereafter 885) (Figure 1A), a small-molecule degrader of GSPT1,[19] phenocopied the effect of 103 (Figure 2G). Given that GSPT1 is a critical component of the translation machinery, its depletion is likely to affect cellular proteostasis. Indeed, as previously reported,[20] GSPT1 degradation promoted by CC-885 led to induction of integrated stress response (ISR) and resulted in global inhibition of translation. We therefore asked if the anti-IAV effect of 103 was a direct consequence of impaired translation termination or an indirect consequence of global translation inhibition.

We first determined whether 103-induced GSPT1 depletion induces the ISR in A549 cells. Contrary to previous reports,[20] we found that levels of both total eIF2α (eukaryotic initiation factor 2; encoded by EIF2S1) and phosphorylated eIF2α (p-eIF2α) were reduced in A549 cells upon 103 treatment (Figure 2G). This effect was not specific to 103, as similar reductions were seen in 885-treated cells (Figure 2G). This decrease was dependent on GSPT1 degradation, as no changes in either eIF2α or p-eIF2α was observed in inactive 96- and 142-treated cells (Figure 2G). eIF2α is a subunit of eIF2 (translation initiation factor 2), which catalyzes the first step of translation initiation. Unsurprisingly, downregulation of eIF2α reduces overall protein synthesis. This mechanism is thought to be important for conferring pro-survival and anti-apoptotic effects under conditions of ER stress.[21] Our observations, that total eIF2α and p-eIF2α are downregulated upon the treatment of 103, suggest that both translation termination and translation initiation are impaired by GSPT1 degradation.

103-induced degradation of GSPT1 confers anti-IAV effect

We next addressed the relationship between 103-induced GSPT1 degradation and IAV replication in a time-of-addition experiment. As demonstrated in a plaque assay (Figure 3A), stronger anti-IAV activity was elicited when GSPT1 in A549 cells was degraded “early” by treating 103 to cells at time points (−3h to +2h) relative to infection (0h). Notably, the antiviral effect of 103 was tunable upon washout (Figure 3B) likely due to the quick recovery of GSPT1 level. Additionally, *CRBN* silencing in A549 cells by genetic interference approach greatly mitigated the antiviral potency of 103 against WT PR8 virus replication in A549 cells (Figure 3C), which implicates that the recruitment of CRBN is critically needed for 103 to confer the anti-IAV potency.

We then used chemical disruption strategy to further investigate this correlation. Since concurrent treatments with Lenalidomide, MLN4924, or MG-132 entirely prevented GSPT1 from being degraded following the treatment of 103 in A549 cells (Figure 2E), we co-treated cells with 103 and these chemical competitors to see if the co-treatment could debilitate the anti-IAV effect of 103. As expected, co-treatments largely compromised the anti-IAV potency of 103 (Figure 3D). These data indicate that CRBN involvement, NEDD8 conjugation, and proteasomal degradation all contribute to the anti-IAV effect of 103. Consistently with previous reports from us and others,[22–25] we observed that Lenalidomide, MLN4924, and MG-132 can potentially exert anti-IAV potency (Figure 3D). Moreover, the compound 96 and 142 had no inhibitory potential on the replication of WT PR8 virus in A549 cells (Figure 3E). In contrast, 885 exerted nearly the same degree of anti-IAV potency as 103 (Figure 3E).[19]

We next asked if translation termination impairment or translation initiation shutdown is the determinant of 103’s activity against IAV. We knocked down both *GSPT1* and *ETF1* by siRNA in A549 cells to see if the anti-IAV effect of 103 could be observed. Unexpectedly, simultaneous silencing of these two genes did not significantly inhibit the replication of WT PR8 virus in A549 cells. However, siRNA-mediated knockdown of *EIF2S1* recapitulated the anti-IAV effect of 103 (Figure 3F), indicating that the downregulation of eIF2α, and not the loss of GSPT1/eRf1 complex, causes inhibition of WT PR8 virus replication in A549 cells.

Altogether, our data indicate that 103 exerts its anti-IAV activity by inhibiting translation initiation caused by selective degradation of GSPT1 in A549 cells.

103 elicits anti-IAV activity in lung organoid model

We next asked if 103 could retain anti-IAV activity in physiologically relevant models.[26] We first tested the effect of 103 on IAV replication in epithelial cells from lung organoids derived from human pluripotent stem cells (hPSCs). 103 treatment strongly inhibited the replication of NS1-GFP PR8 virus in pre-differentiated cells within 24 hours (Figure 4A, left and middle), whereas it did not significantly reduce cell viability in uninfected cells (Figure 4A, middle, Figure S1A). As expected, 103's anti-IAV effect, shown by the dramatically decreased level of NP in the infected cell lysates, was correlated with the degradation of GSPT1/eRF1 complex and the downregulation of eIF2α (Figure 4A, right). Comparable results were also obtained when we tested the anti-IAV potency of 103 in three-dimensional (3D) lung organoid cultures. As demonstrated in immunofluorescence staining, NP level in the WT PR8 virus-infected organoids was decreased following 103 treatment compared to DMSO treatment (Figure 4B). Taken together, our data suggest that 103 is able to elicit great anti-IAV potency even in non-transformed, physiologically, and structurally relevant human models.

103 has antiviral activity against SARS-CoV-2 and CMV

Given the central roles of GSPT1 and eIF2α respectively in regulating translation termination and translation initiation,[18,27] we hypothesized that 103 could hinder the replication of viruses belonging to different viral families. We thus started by examining the GSPT1-depletion-dependent inhibitory potential of 103 on the replication of SARS-CoV-2 in A549 cells that stably express human ACE2 (angiotensin-converting enzyme 2), the receptor for SARS-CoV-2 infection, (A549-ACE2).[28] 103 restricted the replication of SARS-CoV-2 in A549-ACE2 cells throughout infection and displayed negligible cytotoxicity (Figure 5A, top, Figure S1A). The anti-SARS-CoV-2 effect of 103 was correlated with the degradation of GSPT1 and downregulation of eIF2α (Figure 5A, bottom). Nucleozin, as expected, did not exhibit any anti-SARS-CoV-2 effect (Figure 5A).

We then performed whole-cell proteomic analysis. In A549-ACE2 cell lysates treated with 103 for 4 hours, GSPT1 was the most abundantly degraded protein (Figure 5B, top, and Supplementary Table 2). In A549-ACE2 cell lysates infected with SARS-CoV-2 and treated with 103, all the viral proteins and GSPT1 were significantly reduced (Figure 5B, middle and bottom, Figure S3, and Supplementary Table 2). Similar to the anti-IAV effect (Figure 3A), depletion of GSPT1 by 103 before infection conferred a much more potent anti-SARS-CoV-2 activity (Figure 5B, middle and bottom, Figure S3, and Supplementary Table 2). ACE2 levels in A549-ACE2 cells were unaltered by 103 (Figure 5A, Figure S3 and Supplementary Table 2), ruling out the possibility that the anti-SARS-CoV-2 effect of 103 was achieved via interfering with changes in expression of the cell receptor.

Next, we evaluated whether CRBN engagement is strictly required for 103 to exert anti-SARS-CoV-2 activity. Knocking down *CRBN* in A549-ACE2 cells by siRNA largely alleviated the degradative effect of 103 on GSPT1 and the reduction of eIF2α level

(Figure 5C, bottom). Therefore, the antiviral potency of 103 against SARS-CoV-2 infection was significantly debilitated (Figure 5C, top). These data support the notion that CRBN participation is essential for the anti-SARS-CoV-2 effect of 103. Moreover, as expected, 103 exhibited significant anti-SARS-CoV-2 activity in 3D lung organoid cultures (Figure 5D).

We then assessed the antiviral activity of 103 against human cytomegalovirus (CMV). By utilizing $AD169^{BADrUL131}$ virus, a recombinant CMV expressing GFP,[29] we determined that 103 is capable of inhibiting CMV replication in ARPE-19 cells (an immortalized human retinal pigment epithelial cell line) with little effect on cell viability (Figure 6A, left and middle, Figure S1A). Furthermore, similar level of anti-CMV potency of 103 was also observed in primary normal human dermal fibroblasts (NHDF) (Figure S4, left and middle, Figure S1A). As expected, the antiviral effect of 103 against CMV (Figure 6A and Figure S4, left and middle) was correlated with the loss of GSPT1/eRf1 complex in human cells (Figure 6A and Figure S4, right). However, differently from what we observed in A549 cells (Figure 2G, right), lung organoid-derived epithelial cells (Figure 4A, right), and A549-ACE2 cells (Figure 5A, bottom), 103 induced ISR in ARPE-19 cells and NHDF by promoting the phosphorylation of eIF2α while maintaining the constant level of eIF2α (Figure 6A and Figure S4, right). For all these events, the CRBN involvement is indispensable (Figure 6B).

Altogether, by promoting the depletion of GSPT1, 103 can effectively protect human cells from infection by multiple divergent species of viruses.

TPD promoted by RNA mimics exhibits anti-IAV potency

Other than choosing small molecules as ligands targeting viral proteins for constructing PROTAC modalities, we incorporated RNA oligonucleotides into PROTAC design for pursuing virus-specific antivirals. We chose to use the untranslated region (UTR) of IAV RNAs as our initial model system. The rationale of this design is that IAV 5’ and 3’ UTRs function as promoters and recruit viral polymerase (vPOL) for viral RNA (vRNA) transcription and replication. The UTRs of each vRNA segment have been shown to be highly conserved within each segment and have lower evolutionary rates, relative to the coding sequences of the virus (Figure 7A, Figure S5A).[30,31] These sequences are also highly conserved between genomic segments, viral strains and host organisms (Figure 7A, Figure S5A). Given their roles in vPOL recruitment and their high conservation levels, we hypothesized that these sequences can be utilized as excellent ligands for designing antiviral molecules.

We first designed and generated four biotinylated RNA oligonucleotides that bear the sequences of the first 15 bases of the NP vRNA segment of WT PR8 virus (RNA3 and RNA4) and their reverse complementary sequences (RNA1 and RNA2) (Figure 7B, Figure S5B). The first nucleotides of Biotin-RNA1 and 4 were monophosphorylated in order to mimic the natural substrate of vPOL.[32] As verified in a pull-down assay, all 4 Biotin-RNAs were able to bind vPOL complex from WT PR8 virus-infected cell lysates, as quantified by the abundance of NP, a component of the viral ribonucleoprotein (RNP) complex. No Biotin-RNAs could pull down another well-characterized RNA-binding protein NS1[33] or housekeeping protein GAPDH (Figure 7C), supporting the specificity of our assay. On the basis of this set of data, RNA3 and 4, which correspond to genomic vRNA sequences,

were selected as RNA oligonucleotide-based ligands for vPOL to build heterobifunctional molecules. We labeled these molecules “Destroyers”. Two Destroyers, RNA3-A and RNA4-A, were synthesized by conjugating of RNA3 and RNA4 with AHPC, a common ligand for E3 ligase VHL (Figure 7B, Figure S5B). 2’-O-methyl nucleobases and phosphorothioate backbones were used for increasing oligonucleotide stability and enhancing nuclease resistance in the cells.[34] Structural analysis suggests that the conjugation with AHPC is unlikely to disrupt the binding between RNA3/RNA4 and vPOL (Figure 7D).

We next verified if Destroyers could indeed serve as a bridge between vPOL and AHPC. We first generated lysates from A549 cells infected with a recombinant IAV carrying a FLAG tag in the PB1 segment (FLAG-PB1 PR8 virus).[25] The lysates were then incubated with and without RNA3-A/RNA4-A. We then immunoprecipitated the PB1 subunit of vPOL. We reasoned that if the Destroyers function as *bona fide* heterobifunctional molecules, we would then expect them to stabilize protein-protein interactions between vPOL and VHL. Indeed, VHL was selectively co-immunoprecipitated with PB1 in the presence of RNA3-A and RNA4-A (Figure 7E).

We then evaluated anti-IAV activity of Destroyers by using flow cytometry in tandem with NS1-GFP PR8 virus. As exhibited in Figure 7F, both RNA3-A and RNA4-A significantly inhibited the fluorescence intensity levels of NS1-GFP in the infected HEK293T cells, compared to untreated cells. This inhibition was dependent on the active proteasome (Figure 7F). Additionally, RNA4-A displayed a much greater inhibition of NS1-GFP levels than RNA3-A (Figure 7F). Introduction of synthetic oligonucleotides in cells have been shown to potentiate inflammatory responses.[35,36] To determine if this contributes to the antiviral activities of Destroyers, we asked if RNA3-A or RNA4-A is able to induce Type I interferon signaling in uninfected cells. As evaluated by RT-PCR, compared to untreated cells, treatment of cells with RNA4-A significantly upregulated the transcription of interferon-β, whereas RNA3-A did not (Figure S5C). This suggests that the stronger potency of RNA4-A compared to RNA3-A (Figure 7F) may be partially attributed to increased interferon levels in cells.

Taken together, our data suggest that Destroyers can potentially act as heterobifunctional molecules to target vPOL for degradation and confer antiviral activity.

DISCUSSION

Due to many inherent advantages of PROTAC,[5] this strategy has been primarily developed in the context of anticancer therapeutics in the past 20 years.[7] However, substantial exploration of the PROTAC paradigm in seeking antiviral therapies remains marginal. In this study, we provide evidence that targeted protein degradation can be extensively and deeply explored for pursuing innovative chemical modalities against viral infections. We conducted this study by selecting both small molecules and RNA oligonucleotides as ligands to construct and identify antiviral therapeutics.

TPD of GSPT1 as an antiviral therapeutic strategy against IAV

A whole-cell phenotypic screening led us to serendipitously identify a small-molecule degrader of human GSPT1, 103, that can inhibit the replication of IAV in human cells. Since viral replication is highly reliant on the protein synthesis machinery in the host cells, many factors at the stages of initiation, elongation and termination during the process of translation have been validated as targets for developing antiviral drugs.[37] Human *GSPT1* was originally characterized as an essential gene for the G1-to-S phase transition of the cell cycle and was subsequently validated to encode a protein that functions as a peptide chain release factor, eRF3a, for regulating the termination of protein biosynthesis.[18,38] It was found in recent studies that targeting GSPT1 for degradation led to ISR pathway activation and further translation initiation inhibition.[39,40]

103-induced GSPT1 depletion resulted in protein synthesis shutdown via downregulating the level of eIF2α or inducing the phosphorylation of eIF2α, depending on the cell types. Downregulation of eIF2α appears to be specific to and necessary for the antiviral activity of 103 against IAV. Overall, 103's anti-IAV activity is attributable to both translation termination impairment and translation initiation inhibition.

TPD of GSPT1 as a pan-viral antiviral therapeutic

Previous reports suggest that human GSPT1 directly interacts with the viral polymerases of Ebola virus (EBOV) and Lassa virus (LASV).[41,42] In this study, TPD of GSPT1 confers antiviral activity against IAV, SARS-CoV-2, and CMV. As GSPT1 has not been previously reported to significantly interact with the proteomes of the latter viruses,[25,43,44] we surmise that 103 is predominantly acting as a host-directed antiviral therapeutic in the context of these infections. Aside from providing clear evidence-of-concept that PROTAC approach is feasible to be utilized in antiviral treatment, our data also support the idea that controlling protein expression and apical trafficking is a valuable pan-viral host-directed therapy.[45,46] In support of this, we have also previously shown that CT8, a specific inhibitor of SEC61A1, a factor controlling cotranslational translocation of proteins across ER, impairs the replication of IAV, human immunodeficiency virus (HIV) and dengue virus (DENV) infections.[25]

103 has been validated to possess broad-spectrum antiviral potency. In a similar manner, previously reported GSPT1 degraders, such as CC-885,[19] could also be repurposed for treating viral infections. Moreover, CC-90009, a GSPT1-selective cereblon E3 ligase modulating (CELMoD) agent, has entered clinic trials for treating patients with acute myeloid leukemia (AML),[39,40] which paves a path for applying GSPT1-deletion-based strategies to treat viral infections. Further exploration and studies are needed to understand the therapeutic potential of GSPT1 degraders as pan-antivirals.

Viral RNA mimics as ligands for TPD

Compared to small molecules, RNA oligonucleotides have multiple favorable properties to be chosen as the ligands in designing PROTAC modalities, especially when targeting RNA-binding proteins with very high sequence-specific binding. For example, RNA oligonucleotides can maintain high affinity with vPOL while providing easy access to synthesis and purification. In addition, this type of ligand requires minimal design and

only the sequences of the target viral genomic regions. As a potential therapeutic, this is attractive as it confers a high level of adaptability to the molecules, allowing for the speedy modification of sequences if viral target sequences acquire genomic mutations.

While the effects we observed with Destroyers are modest, this proof-of-concept research is encouraging. **Further effort will be focused on validating the direct degradation of vPOL by Destroyers.** In addition, future improvements should take into consideration the optimization of the sequences of Destroyers with respect to their specificity, pharmacokinetic properties, and immunogenicity, which are highly dependent on sequence composition, length and backbone and sugar chemistry. Indeed, despite very similar sequence compositions, two Destroyers identified in this this study have differing ability to induce Type I interferon signaling, which likely contributes to the differences in their antiviral efficacies. This might be in part related to our use of a phosphorothioate backbone, which has been shown to be immunostimulatory in a sequence-specific manner.[47–49] In theory, having an RNA-based molecule that induces antiviral responses and targets viral proteins for degradation could be useful, like in many instances in which viral antagonists elicit suppression of antiviral response. This, of course, needs always to be considered with respect to viral pathogenesis, and tested in vivo.

In addition to optimization of the oligonucleotide-based ligands, it would also be important to further optimize E3 ligases for targeting viral proteins. Many viruses have co-evolved mechanisms to hijack the host UPS, so it is not a given that such strategy would work for all E3 ligases.

The need for next-generation antivirals

The recent global pandemic has highlighted the extremely urgent need for innovative antiviral agents.[50] To address this unprecedented challenge, in this proof-of-concept study, we demonstrate that PROTAC approach as an exemplary TPD strategy that has been widely exploited in the field of cancer research can be utilized in seeking antivirals as well. Identification of small-molecule degrader 103 and Destroyer RNA3-A suggests that there is room for developing and rationally design antivirals using the PROTAC platform.

LIMITATIONS OF STUDY

We have presented proof-of-concept that TPD can be exploited to develop both host-directed and virus-specific strategies against viral infections. Our data suggest that at the doses and short time frames we utilized, the replication of IAV, SARS-CoV-2 and CMV are sensitive to 103-mediated translation inhibition, while host cells are tolerant with minimal cytotoxic effects. However, as a host-directed strategy targeting proteostasis, further evaluation of the long-term pharmacokinetics and toxicity profiles of 103 in an *in vivo* context is still necessary. In this study, in vivo validation is limited by lack of effective *in vivo* animal models for validating these strategies. This is especially true for phthalimide-based PROTAC molecules. For instance, phthalimide derivatives are difficult to be evaluated in mice because of species-specific differences in murine CRBN that render it resistant to this type of molecules.[51] Even in the humanized cereblon ($CRBN^{I391V}$) mice, phthalimide analogues demonstrated divergent levels of effect in ameliorate dextran sodium sulfate (DSS)-mediated

colitis.[52] Additionally, GSPT1 degraders CC-885 and CC-90009, even with minor structural divergences, required distinct mutations on CRBN ($CRBN^{V380E}$ and $CRBN^{V380E\ and\ I391V}$) in mice.[20] Validation of 103 in the case of respiratory viral infection has thus primarily been performed in the context of xenograft models in this study.

On the other hand, our study of Destroyers is limited by the lack of delivery efficiency. Although RNA-based therapies, such as antisense oligonucleotides, have lately revolutionized the treatment of neurodegenerative diseases, such as spinal muscular dystrophy, the delivery of oligonucleotides at effective concentrations to extrahepatic tissues *in vivo*, such as lung, remains a major limitation.[53] Current methods of oligonucleotide delivery most likely have to be modified in order to assess Destroyers *in vivo*. Moreover, Destroyer RNA3-A is with limited configurations in terms of oligonucleotide sequences and their modifications, E3 ligase ligand choices, and linker structures. Further iterative refinements would, in principle, expand and improve specificity and activity of Destroyers.

STAR METHODS

RESOURCE AVAILABILITY

Lead Contact—Further information and requests for reagents may be directed to and will be fulfilled by Lead Contact Ivan Marazzi (imarazzi@uci.edu).

Materials Availability—All unique/stable reagents generated in this study are available from the Lead Contact with a completed Materials Transfer Agreement.

Data and Code Availability

- Proteomics data have been deposited at PRIDE and is publicly available as of the date of publication. Accession numbers are listed in the key resources table. Supplemental Items are available from Mendeley Data at http://dx.doi.org/10.17632/6k6ng65623.1
- This paper does not report original code
- Any information required to reanalyze the data reported in this paper is available from the lead contact upon request.

EXPERIMENTAL MODEL AND SUBJECT DETAILS

Cell cultures—Human alveolar basal epithelial carcinoma cells (A549 and A549-ACE2), Human embryonic kidney cells (HEK293T), Madin-Darby canine kidney cells (MDCK), and monkey kidney epithelial cells (Vero E6), Primary Normal Human Dermal Fibroblasts (NHDF) were all cultured in DMEM supplemented with 10% FBS and 10% antibiotic-antimycotic at 37 °C and 5% CO_2. Human Bronchial/Tracheal Epithelial Cells (HBTE) were cultured in airway epithelial cell basal medium (ATCC PCS-300–030) supplemented with bronchial epithelial cell growth kit (ATCC PCS-300–040) at 37 °C and 5% CO_2. Human retinal epithelial cells (ARPE-19) were cultured in DMEM and Ham's F-12 Nutrient Mix at 1:1 ratio supplemented with 10% FBS, 25 mM HEPES, and 10% antibiotic-antimycotic at 37 °C and 5% CO_2.

hPSC derived lung organoid cultures—Lung organoids were generated from human pluripotent stem cells (hPSCs) and validated as previously described.[26] Briefly, hPSC differentiation into endoderm was performed in serum-free differentiation (SFD) medium of IMDM/Ham's F-12 (3:1) supplemented with the following: 1X N-2 supplement, 0.5 x B-27™, 50 μg/mL L-ascorbic acid, 1X GlutaMAX™ Supplement, 0.45 mM monothioglycerol, 0.05% BSA, 10 μM Y-27632, 0.5 ng/mL human bone morphogenetic protein 4, 2.5 ng/mL human basic fibroblast growth factor, and 100 ng/mL human Activin A, in a 5% CO_2/5% O_2 atmosphere at 37 °C for 72–76 hours.

On Day 4, endoderm yield was determined by the expressions of C-X-C chemokine receptor type 4 and c-KIT by flow cytometry. Cells used in all experiments had > 90% endoderm yield. For induction of anterior foregut endoderm, embryonic bodies were dissociated into single cells using 0.05% trypsin/0.02% EDTA and plated onto fibronectin-coated, 6-well tissue culture plates (80,000–105,000 cells/cm^2). Cells were incubated in SFD medium supplemented with 100 ng/mL human NOGGIN and 10 μM SB431542 for 24 hours followed by switching to SFD media supplemented with 10 μM SB431542 and 1 μM IWP 2 for another 24 hours.

At the end of anterior foregut endoderm induction, cells were treated with SFD media supplemented with the following: 3 μM CHIR 99021, 10 ng/mL human fibroblast growth factor 10, 10 ng/mL human keratinocyte growth factor, 10 ng/mL human BMP4 and 50nM all-trans retinoic acid for 48 hours, and three-dimensional clump formation was observed. The clumps were then suspended by gently pipetting around the wells. The suspended clumps were maintained in ultra-low attachment multiple-well plates submerged in CFKBRA medium and were fed every other day until day 20 to day 25. Lung organoids were either kept in low attachment plates (hereby refer as suspension culture) or embedded in Matrigel to induce the branching morphogenesis (hereby refer as 3D culture). On Day 20-Day 25, lung organoids were embedded in 100% Matrigel in 24-well Transwell inserts to generate branching morphogenesis. Media were changed every other day. The 3D cultures were maintained until Day 50 for virus infection and compound treatment.

For epithelial cells derived from lung organoids, suspension cultures from Day 35 to Day 60 were dissociated into single cells using TrypLE™ Express Enzyme. Cells were seeded at 20,000–50,000 cells per well in 96-well plate or 100,000–200,000 cells per well in 24-well plate coated with fibronectin. Cells were cultured in CFKBRA medium supplemented with Rock inhibitor for 24 hours before viral infection and compound treatment.

METHODS DETAILS

Section I Small-molecule degrader

Synthesis of compound FM-74–103, FM-123–96 and FM-123–142: All chemical reagents were purchased from commercial vendors and used without further purification. Preparative high-performance liquid chromatography (HPLC) for purifying the compounds was conducted by using an Agilent Prep 1200 series with a Phenomenex Luna 75×30 mm 5 μm C18 column. Analytic HPLC for determining the purity of compounds was performed by using an Agilent 1200 Series system with a Zorbax 300SB-C18 2.1×150 mm 5 μm column.

Ultra performance liquid chromatography (UPLC) for determining the purity of compounds was performed by using a Waters Acquity I-Class UPLC system with a ACQUITY UPLC BEH C18 2.1×30 mm 1.7 μm column. Nuclear magnetic resonance (NMR) data were acquired by using a Bruker DRX-600 spectrometer (600 MHz for proton, ^{1}H NMR; 151 MHz for carbon, ^{13}C NMR). High-resolution mass spectra (HRMS) data were acquired by using Agilent G1969A API-TOF with an electrospray ionization (ESI) source.

Reagents and conditions: A) BBr_3, DCM, room temperature, overnight; B) 4-Pentyn-1-ol, $Pd(PPh_3)_2Cl_2$, CuI, DMF, NEt_3, 90 °C, overnight; C) Pd/C, H_2, MeOH, room temperature, 6 hours; D) MsCl, NEt_3, DCM, DMF, room temperature, 1 hour; E) Phenol, K_2CO_3, NaI, DMF, 65 °C, overnight; F) $NaHCO_3$, NaI, DMF, 80 °C, overnight.

(4-(2-chloro-4-nitrophenyl)piperazin-1-yl)(3-(2-methoxyphenyl)-5-methylisoxazol-4-yl)methanone (1): Compound **1** was synthesized according to the previously published procedure.[59]

(4-(2-chloro-4-nitrophenyl)piperazin-1-yl)(3-(2-hydroxyphenyl)-5-methylisoxazol-4-yl)methanone (2): To a solution of BBr_3 (2.5 mL of 1 M solution, 2.5 mmol) in DCM (20 mL) were added compound **1** (456 mg, 1mmol) in DCM (10 mL) slowly at −78 °C. The mixture was stirred at room temperature overnight. Upon completion, aqueous solution of $NaHCO_3$ was added to the solution. The mixture was then extracted with DCM (30 mL×3). The combined organic layers were dried over Na_2SO_4 and then filtered. The mixture was purified by preparative HPLC to afford compound **2** as yellow solid (400 mg, 91% yield).

^{1}H NMR (600 MHz, DMSO-d_6) δ 10.01 (s, 1H), 8.26 (d, J = 2.7 Hz, 1H), 8.20 (dd, J = 9.0, 2.7 Hz, 1H), 7.41 (dd, J = 7.5, 1.7 Hz, 1H), 7.32 (ddd, J = 8.9, 7.3, 1.8 Hz, 1H), 7.24 (d, J = 9.0 Hz, 1H), 6.91 (dd, J = 9.9, 7.9 Hz, 2H), 3.70 (s, 2H), 3.48 (s, 2H), 3.21 (s, 2H), 2.96 (s, 2H), 2.48 (s, 3H).

MS (ESI) $[M + H]^+$ = 443.2.

3-(5-(5-hydroxypentyl)-1-oxoisoindolin-2-yl)piperidine-2,6-dione (4, FM-123–96): A mixture of compound **3** (830 mg, 2.57 mmol), 4-Pentyn-1-ol (220 mg, 2.57 mmol), $Pd(PPh_3)_2Cl_2$ (180 mg, 0.257 mmol), and CuI (100 mg, 0.514 mmol) in DMF (6 mL) and NEt_3 (3 mL) was stirred at 90 °C overnight. Upon completion, the DMF was removed by preparative HPLC to afford a crude intermediate (1.1 g), which was used for the next step without further purification.

The crude intermediate (230 mg) was dissolved in MeOH (20 mL). To the solution was added Pd/C (90 mg). The mixture was stirred under H_2 atmosphere at room temperature for 6 hours. Upon completion, the Pd/C was removed by filtration and the residue was purified by preparative HPLC to afford compound **4** (FM-123–96) as yellow solid (210 mg, 91% yield).

^{1}H NMR (600 MHz, Acetone-d_6) δ 9.77 (s, 1H), 7.70 (d, J = 7.8 Hz, 1H), 7.47 (s, 1H), 7.40 (dd, J = 7.7, 1.4 Hz, 1H), 5.22 (dd, J = 13.4, 5.2 Hz, 1H), 4.54–4.43 (m, 2H), 3.57 (t, J =

6.5 Hz, 2H), 3.03 (ddd, *J* = 17.5, 13.7, 5.4 Hz, 1H), 2.85–2.76 (m, 3H), 2.64–2.53 (m, 1H), 2.27–2.19 (m, 1H), 1.77–1.69 (m, 2H), 1.64–1.53 (m, 2H), 1.49–1.42 (m, 2H).

MS (ESI) $[M + H]^+$ = 331.2.

5-(2-(2,6-dioxopiperidin-3-yl)-1-oxoisoindolin-5-yl)pentyl methanesulfonate (5): To a solution of compound **4** (260 mg, 0.79 mmol) in DCM (10 mL) and DMF (2 mL) was added MsCl (108 mg, 0.95 mmol) and NEt_3 (0.16 mL, 1.18 mmol) at 0 °C. The mixture was stirred at room temperature for 1 hour. Upon completion, the mixture was purified by preparative HPLC to afford compound **5** as white solid (160 mg, 50% yield).

^{1}H NMR (600 MHz, Methanol-d_4) δ 7.75 (d, *J* = 7.8 Hz, 1H), 7.49 (s, 1H), 7.43 (dd, *J* = 7.9, 1.4 Hz, 1H), 5.18 (dd, *J* = 13.3, 5.2 Hz, 1H), 4.53 (d, *J* = 16.9 Hz, 1H), 4.46 (d, *J* = 16.9 Hz, 1H), 4.27 (t, *J* = 6.4 Hz, 2H), 3.09 (s, 3H), 2.95 (ddd, *J* = 17.6, 13.6, 5.4 Hz, 1H), 2.85–2.80 (m, 2H), 2.82–2.76 (m, 1H), 2.52 (qd, *J* = 13.3, 4.5 Hz, 1H), 2.23–2.16 (m, 1H), 1.86–1.73 (m, 4H), 1.55–1.47 (m, 2H).

MS (ESI) $[M + H]^+$ = 409.1.

3-(1-oxo-5-(5-phenoxypentyl)isoindolin-2-yl)piperidine-2,6-dione (6, FM-123–142): A mixture of compound **5** (10 mg, 0.025 mmol), phenol (5 mg, 0.5 mmol), K_2CO_3 (11 mg, 0.08 mmol) and NaI (7.5 mg, 0.05 mmol) in DMF (1 mL) was stirred at 65 °C overnight. Upon completion, the mixture was purified by preparative HPLC to afford compound **6** (FM-123–142) as white solid (3.75 mg, 38% yield).

^{1}H NMR (600 MHz, Acetone-d_6) δ 9.77 (s, 1H), 7.70 (d, *J* = 7.8 Hz, 1H), 7.49 (s, 1H), 7.42 (d, *J* = 7.7 Hz, 1H), 7.33–7.27 (m, 2H), 6.96–6.91 (m, 3H), 5.22 (dd, *J* = 13.3, 5.2 Hz, 1H), 4.51 (d, *J* = 16.5 Hz, 1H), 4.45 (d, *J* = 16.5 Hz, 1H), 4.03 (t, *J* = 6.4 Hz, 2H), 3.03 (ddd, *J* = 17.3, 13.7, 5.4 Hz, 1H), 2.86–2.78 (m, 3H), 2.59 (qd, *J* = 13.3, 4.5 Hz, 1H), 2.27–2.20 (m, 1H), 1.90–1.76 (m, 4H), 1.66–1.54 (m, 2H).

MS (ESI) $[M + H]^+$ = 407.1.

3-(5-(5-(2-(4-(4-(2-chloro-4-nitrophenyl)piperazine-1-carbonyl)-5-methylisoxazol-3-yl)phenoxy)pentyl)-1-oxoisoindolin-2-yl)piperidine-2,6-dione (7, FM-74–103): A mixture of compound **2** (11 mg, 0.025 mmol), compound **5** (13.3 mg, 0.0325 mmol), $NaHCO_3$ (8.4 mg, 0.1 mmol) and NaI (7.5 mg, 0.05 mmol) in DMF (1.5 mL) was stirred at 80 °C overnight. Upon completion, the mixture was purified by preparative HPLC to afford compound **7** (FM-74–103) as yellow solid (11.9 mg, 63% yield).

^{1}H NMR (600 MHz, Acetone-d_6) δ 9.77 (s, 1H), 8.23 (d, *J* = 2.6 Hz, 1H), 8.16 (dd, *J* = 8.9, 2.7 Hz, 1H), 7.68 (d, *J* = 7.8 Hz, 1H), 7.58–7.50 (m, 2H), 7.45 (s, 1H), 7.39 (d, *J* = 7.7 Hz, 1H), 7.20 (d, *J* = 8.3 Hz, 1H), 7.15–7.10 (m, 2H), 5.22 (dd, *J* = 13.4, 5.2 Hz, 1H), 4.50 (d, *J* = 16.5 Hz, 1H), 4.45 (d, *J* = 16.4 Hz, 1H), 4.08 (t, *J* = 6.7 Hz, 2H), 3.86–3.64 (m, 4H), 3.32–3.08 (m, 4H), 3.03 (ddd, *J* = 17.4, 13.7, 5.4 Hz, 1H), 2.84–2.77 (m, 3H), 2.63–2.54 (m, 1H), 2.54 (s, 3H), 2.23 (dtd, *J* = 12.9, 5.3, 2.4 Hz, 1H), 1.85 (p, *J* = 6.9 Hz, 2H), 1.75 (p, *J* = 7.6 Hz, 2H), 1.48 (tt, *J* = 9.3, 6.4 Hz, 2H).

^{13}C NMR (151 MHz, Acetone-*d*6) δ 171.8, 170.4, 170.3, 168.3, 162.4, 158.6, 157.2, 154.5, 147.1, 142.7, 142.5, 131.6, 130.7, 129.9, 128.3, 127.2, 126.0, 123.5, 123.2, 123.0, 120.7, 120.3, 118.3, 112.8, 112.3, 68.5, 51.8, 50.1, 46.9, 35.6, 31.3, 31.0, 29.7, 28.2, 25.3, 23.1, 11.0. HRMS calculated for $C_{39}H_{40}ClN_6O_8$ $[M + H]^+$ 755.2591, found 755.2610.

Compound treatment: A549 cells were seeded in 6-well plates (90% confluence) one day before compound treatment. On the day of compound treatment, cell culture medium was first changed.

In the assays of validating the degradation of IAV NP, 10 mM DMSO stocks of the indicated compounds were added into the medium (working concentrations = 1 μM, 0.1% DMSO) at 0 hour or 24 hours post the DNA transfection. A549 cells were incubated with the compounds at 37 °C for 24 hours.

In the assays of validating the suppression of expressing the transfected genes, 10 mM DMSO stocks of the indicated compounds were added into the medium (working concentrations = 1 μM, 0.1% DMSO) at 0 hour post the DNA transfection. A549 cells were incubated with the compounds at 37 °C for 24 hours.

In the assays of validating the time- and concentration-dependent degradation of GSPT1, 10 mM DMSO stocks of the indicated compounds were added into the medium to achieve the indicated working concentrations. A549 cells were incubated with the compounds at 37 °C for the indicated periods of time.

In the assays of validating the reversible degradation of GSPT1, 10 mM DMSO stock of 103 was added into the medium (working concentrations = 0.1 μM, 0.1% DMSO). A549 cells were incubated with 103 at 37 °C for 24 hours. The medium containing 103 was removed and fresh medium was added back. A549 cells were cultured in the fresh medium at 37 °C for the indicated periods of time.

In competition assays, 10 mM DMSO stocks of the indicated competitor compounds were added into the medium (working concentrations = 10 μM, 0.1% DMSO). A549 cells were incubated with the competitor compounds at 37 °C for 1 hours. 10 mM DMSO stock of 103 was then added into the medium (working concentrations = 1 μM, 0.1% DMSO). A549 cells were incubated with the indicated competitor compounds and 103 at 37 °C for 6 hours.

In RT-PCR assays, 10 mM DMSO stock of 103 was added into the medium (working concentrations = 1 μM, 0.1% DMSO). A549 cells were incubated with 103 at 37 °C for the indicated periods of time.

After compound treatment was completed, fluorescence images were recorded by EVOS Cell Imaging Systems; cell pellets were collected for processing Western Blots and RT-PCR.

Transfection: For DNA transfection, A549 cells were seeded in 6-well plates (70% confluence) one day before transfection. On the day of transfection, cell culture medium was changed and cells were transfected with the indicated DNA plasmids (500 ng/well) using Lipofectamine 3000 Transfection Reagent according to the manufacturer's instructions.

For siRNA transfection, A549 cells, A549-ACE2 cells, or ARPE-19 cells were seeded in 6-well plates (50% confluence) one day before transfection. On the day of transfection, cell culture medium was changed and cells were transfected with 20 μM stocks of the indicated siRNA pools (working concentrations = 100 nM) using Lipofectamine RNAiMAX Transfection Reagent according to the manufacturer's instructions.

Infection

IAV infection of A549 cells and HBTE cells: A549 cells were seeded in 6-well plates (90% confluence) one day before infection. On the day of infection, cell culture medium was removed. A549 cells were washed by PBS and incubated with NS1-GFP PR8 virus or WT PR8 virus diluted in opti-MEM (MOI = 1) (200 μL/well) at 37 °C for 1 hour to allow virus to adsorb. Plates were agitated every 10 minutes during the infection to ensure even distribution of inoculum. No compound is present during the viral adsorption step. After virus adsorption step, infection inoculum was removed. A549 cells were washed by PBS and fresh medium was added back. Addition of fresh medium constitutes the time point of 0 hour post infection. 10 mM DMSO stocks of the indicated compounds were then added into the medium at the indicated time points before or post infection (relative to 0 hour post infection) to achieve the indicated concentrations. A549 cells were then incubated with the compounds at 37 °C for 24 hours.

48-hour siRNA-transfected A549 cells were infected by WT PR8 virus and treated with 103 following the same procedures.

HBTE cells were infected by WT PR8 virus or A/Netherlands/602/2009 (H1N1) virus and treated with 103 following the same procedures.

24 hours post infection, fluorescence images were recorded by EVOS Cell Imaging Systems and the images were analyzed by ImageJ software; cell culture supernatants were saved for processing plaque assays and cell pellets were collected for processing Western Blots.

IAV infection of lung organoid cells: The cells dissociated from lung organoid were seeded in 24-well plates (90% confluence) one day before infection. On the day of infection, cell culture medium was changed and 10 mM DMSO stocks of the indicated compounds were added into the medium (working concentrations = 1 μM, 0.1% DMSO). Cells were incubated with the indicated compounds at 37 °C for 3 hours and the medium containing the compounds was removed. Cells were then washed by PBS and incubated with NS1-GFP PR8 virus diluted in CFKBRA medium (MOI = 1) (200 μL/well) at 37 °C for 1 hour. Plates were agitated every 10 minutes during the infection. After virus adsorption, infection inoculum was removed and fresh medium containing the indicated compounds (working concentrations = 1 μM, 0.1% DMSO) was added back. Cells were then incubated with the compounds at 37 °C for 24 hours. 24 hours post infection, fluorescence images were recorded by EVOS Cell Imaging Systems and the images were analyzed by ImageJ software; cell pellets were collected for processing Western Blots.

IAV infection of lung organoids: Lung organoids were generated and cultured in 24-well Transwell inserts. On the day of infection, medium in both upper and lower chambers of the

Transwell inserts were replaced with medium containing the indicated compounds (working concentrations = 1 μM, 0.1% DMSO). Organoids were incubated with the compounds at 37 °C for 3 hours and the insert medium containing the compounds was removed for viral adsorption. Organoids were then incubated with WT PR8 virus diluted in CFKBRA medium (MOI = 1) (200 μL/well) at 37°C for 1 hour. Agitation of plates was not required. After virus adsorption, infection inoculum was removed and fresh medium containing the compounds (working concentrations = 1 μM, 0.1% DMSO) was added back. Organoids were then incubated with the compounds at 37 °C for 24 hours. 24 hours post infection, organoids were collected for processing immunofluorescent staining.

SARS-CoV-2 infection of A549-ACE2 cells: A549-ACE2 cells were seeded in 12-well plates (90% confluence) one day before infection. On the day of infection, cell culture medium was changed and the stock of SARS-CoV-2 was then added into the medium (MOI = 1). Addition of SARS-CoV-2 to A549-ACE2 cells constitutes the time point of 0 hour post infection. 10 mM DMSO stocks of the indicated compounds were then added into the medium (working concentrations = 1 μM, 0.1% DMSO) at the indicated time points before or post infection (relative to 0 hour post infection). A549-ACE2 cells were then incubated with SARS-CoV-2 and the compounds at 37 °C for 24 hours.

48-hour siRNA-transfected A549-ACE2 cells were infected by SARS-CoV-2 and treated with 103 following the same procedures.

Lung organoids were infected by SARS-CoV-2 and treated with 103 following the same procedures.

24 hours post infection, cell culture supernatants were saved for processing plaque assays and cell pellets were collected for processing Western Blots; organoids were collected for processing immunofluorescent staining.

All experiments were performed in a Biosafety Level-3 Facility.

CMV infection of ARPE-19 cells and NHDF cells: ARPE-19 cells or NHDF cells were seeded in 48-well plates (90% confluence) one day before infection. On the day of infection, cell culture medium was changed and 10 mM DMSO stocks of the indicated compounds were added into the medium (working concentrations = 1 μM, 0.1% DMSO). Cells were incubated with the compounds at 37 °C for 3 hours and the medium containing the compounds was removed for viral adsorption. Cells were then washed by PBS and incubated with $AD169^{BADrUL131}$ virus diluted in opti-MEM (MOI = 1) (200 μL/well) at 37 °C for 2 hours. Plates were agitated every 20 minutes during the infection. After virus adsorption, infection inoculum was removed and fresh medium containing the compounds (working concentrations = 1 μM, 0.1% DMSO) was added back. Cells were then incubated with the compounds at 37 °C for 24 hours.

The 48-hour siRNA-transfected ARPE-19 cells were infected by $AD169^{BADrUL131}$ virus and treated with 103 following the same procedures.

24 hours post infection, fluorescence images were recorded by EVOS Cell Imaging Systems and the images were analyzed by ImageJ software; cell pellets were collected for processing Western Blots.

Plaque assay: To quantify the titers of WT PR8 virus in the saved A549 or HBTE cell culture supernatants or A/Netherlands/602/2009 (H1N1) virus in the saved HBTE cell culture supernatants, MDCK cells were seeded in 6-well plates (100% confluence) one day before infection. On the day of infection, cell culture medium was removed. MDCK cells were washed by PBS and incubated with 10-fold serially diluted virus solutions in opti-MEM at 37 °C for 1 hour. Plates were agitated every 10 minutes during the infection. After virus adsorption, infection inoculum was removed MDCK cells were washed by PBS and overlaid with agar/medium mixture (DMEM supplemented with 3.7% $NaHCO_3$, 0.8% agar, 25 mM HEPES, 1 mM sodium pyruvate, 1×penicillin-streptomycin-glutamine, 1× glutamine, and 1 μg/mL TPCK-treated trypsin, pH = 7.0). Plates were incubated at 37 °C for 72 hours. MDCK cells were fixed by 1% formaldehyde and stained by crystal violet solution at room temperature for 1 hour, respectively. Plaques were counted and plaque-forming units (PFU/mL) were calculated.

To quantify the titers of SASR-CoV-2 in the saved A549-ACE2 cell culture supernatants, plaque assays were processed according to the previous protocol.[54] Briefly, Vero E6 cells in 12-well plates (100% confluence) were infected by serially diluted virus solution at 37 °C for 1 hour, washed by PBS, and overlaid with agar/medium mixture (MEM supplemented with 2% FBS, 0.7% agar, 0.2% BSA, 0.12% $NaHCO_3$, 10 mM HEPES, and 4 mM L-glutamine). Plates were incubated at 37 °C for 72 hours. Vero E6 cells were fixed by 10% formalin at room temperature for 24 hours, blotted by anti-SARS-CoV-2 NP and anti-mouse IgG (HRP) at room temperature for 1 hour, respectively. Plaques were finally developed by using the TrueBlue Peroxidase Substrate. Plaques were counted and plaque-forming units (PFU/mL) were calculated.

All experiments were performed in a Biosafety Level-3 Facility.

Western Blot: The collected cell pellets/organoids were boiled in 2x Laemmli sample buffer. The crude cell lysates were separated by SDS-PAGE and proteins were transferred from gels to PVDF membranes. The membranes were incubated in 5% w/v milk in 0.1% Tween-20/PBS at room temperature for 2 hours, incubated with the indicated primary antibodies diluted in 0.1% Tween-20/PBS at 4 °C overnight, and incubated with the indicated secondary antibodies (HRP) diluted in 0.1% Tween-20/PBS at room temperature for 2 hours. The membranes were washed by 0.1% Tween-20/PBS after each incubation. Clarity Western ECL Substrate was applied to the membranes and signal bands were exposed to the X-ray films.

RT-PCR

Total RNAs were extracted from the collected cell pellets by using TRIzol Reagent and converted to cDNA by using High-Capacity cDNA Reverse Transcription Kit. RT-PCR was processed by using iQ SYBR Green Supermix.

Cell viability assay—Cells in 96-well plates (90% confluence) were treated with the indicated compounds at the indicated working concentrations at 37 °C for 24 hours. ATP levels in the cells were quantified by using CellTiter-Glo Luminescent Cell Viability Assay according to the manufacturer's instructions. Metabolic activities in the cells were measured by MTT Assay Kit according to the manufacturer's instructions.

Ubiquitination assays—A549 cells in 6-well plates (90% confluence) were transfected with pCMV6-Entry-FLAG-GSPT1 and pRK5-HA-Ub-WT for 24 hours following the transfection procedures as described above. A549 cells were incubated with DMSO or 1 μM 103 (0.1% DMSO) at 37 °C for 8 hours. Cell pellets were then washed by PBS and suspended in 1 mL lysis buffer (150 mM NaCl, 50 mM TrisHCl pH =7.5, 1 mM EDTA, 0.5% NP40, 1X protease and phosphatase inhibitor) in 5 mL tubes. 50 μL 5M NaCl were added into the tubes and cells were lysed by rotating the tubes at 4 °C for 30 minutes. 1 mL H_2O were added into the tubes. The tubes were rotated at 4 °C for 10 minutes and centrifuged at 15,000 rpm for 10 minutes. The supernatants of the cell lysates were then collected for the pull-down assay.

Pull-down assay was processed according to the manufacturer's instructions of Anti-FLAG M2 Magnetic Beads. Briefly, the pre-washed Anti-FLAG M2 Magnetic Beads were incubated with the supernatants of the cell lysates by gently shaking at 4 °C overnight. The beads were then washed by washing buffer I (150 mM NaCl, 50 mM TrisHCl pH =7.5, 1 mM EDTA) and washing buffer II (150 mM NaCl, 50 mM TrisHCl pH =7.5, 1 mM EDTA, 0.05% NP40). The beads were boiled in 2x Laemmli sample buffer. The eluted samples were collected for processing Western Blots.

Proteomic assay and quantitative analysis—A549 cells or A549-ACE2 cells in 6-well plates were infected by WT PR8 virus or SARS-CoV-2 (MOI = 1) and treated with DMSO or 1 μM 103 (0.1% DMSO) following the infection procedures as described above. Cell pellets were collected, washed by PBS, suspended in the lysis buffer (8M urea, 150 mM NaCl, 50 mM NH_4HCO_3, 1× protease and phosphatase inhibitor), and incubated on ice for 30 minutes.

Lysates were sonicated and protein concentrations were quantified by Micro BCA™ Protein Assay Kit. 50 μg of protein for each sample were treated with 4mM Tris-(2-carboxyethyl)phosphine (TCEP) to reduce disulfide linkages for 30 minutes in the dark at room temperature. 10 mM Iodoacetamide (IAA) was added to alkylate free cysteines and lysates were incubated in the dark at room temperature for 30 minutes. IAA was quenched with 10 mM dithiothreitol (DTT) and samples were incubated in the dark at room temperature for 30 minutes. Samples were then diluted with 5 sample volumes of 100 mM ammonium bicarbonate to reduce the concentration of urea to < 2 M to where trypsin is active. Lysates were next digested with Trypsin Gold at a 1:100 (enzyme: protein) ratio and lysates were rotated for 16 hours at room temperature. Trypsin activity was quenched by adding 10% v/v trifluoroacetic acid (TFA) to a final concentration of 0.1% TFA. Samples were then desalted on a C18 column as per the manufacturer's instructions. Samples were eluted from these columns with 200 μL 40% ACN/0.1% TFA. Samples were dried by vacuum centrifugation.

All samples were analyzed on an Orbitrap Eclipse mass spectrometry system (Thermo Fisher Scientific) equipped with an Easy nLC 1200 ultra-high pressure liquid chromatography system (Thermo Fisher Scientific) interfaced via a Nanospray Flex nanoelectrospray source. Immediately prior to analysis, lyophilized samples were resuspended in 0.1% formic acid. Samples were injected on a C18 reverse phase column (30 cm × 75 μm (ID)) packed with ReprosilPur 1.9 μm particles). Mobile phase A consisted of 0.1% FA, and mobile phase B consisted of 0.1% FA/80% ACN. Peptides were separated by an organic gradient from 5% to 35% mobile phase B over 120 minutes followed by an increase to 100% B over 10 minutes at a flow rate of 300 nL/minute. Analytical columns were equilibrated with 3 μL of mobile phase A. To build a spectral library, replicate samples were pooled by infection and treatment conditions and analyzed by a data-dependent acquisition (DDA) method. DDA data was collected by acquiring a full scan over a m/z range of 375–1025 in the Orbitrap at 120,000 resolution resolving power (@200 m/z) with a normalized AGC target of 100%, an RF lens setting of 30%, and an instrument-controlled ion injection time. Dynamic exclusion was set to 30 seconds, with a 10-ppm exclusion width setting. Peptides with charge states 2–6 were selected for MS/MS interrogation using higher energy collisional dissociation (HCD) with a normalized HCD collision energy of 28%, with three seconds of MS/MS scans per cycle. All individual samples were analyzed by a data-independent acquisition (DIA) method. DIA was performed on all individual samples. An MS scan was performed at 60,000 resolution (@200m/z) over a scan range of 390–1010 m/z, an instrument controlled AGC target, an RF lens setting of 30%, and an instrument controlled maximum injection time, followed by DIA scans using 8 m/z isolation windows over 400–1000 m/z at a normalized HCD collision energy of 28%.

Spectral Libraries were built with Spectronaut factory settings from DDA pools and from DDA runs from a previous SARS-CoV-2 study.[60] Individual samples run with DIA methods were then analyzed against the before mentioned library with Spectronaut as previously described.[61] False discovery rates were estimated using a decoy database strategy.[62] All data were filtered to achieve a false discovery rate of 0.01 for peptide-spectrum matches, peptide identifications, and protein identifications. Search parameters included a fixed modification for carbamidomethyl cysteine and variable modifications for N-terminal protein acetylation and methionine oxidation. All other search parameters were defaults for the respective algorithms. Analysis of protein expression was conducted utilizing the MSstats statistical package in R. Output data from Spectronaut was annotated based on the human reference (SwissProt human reviewed sequences downloaded on 10/10/2019, SARS-CoV-2 (WA1 strain) sequences, and Influenza A virus (PR8 strain) sequences). Technical and biological replicates were integrated to estimate log2fold-changes, p-values, and adjusted p-values. All data were normalized by equalizing median intensities, the summary method was Tukey's median polish, and the maximum quantile for deciding censored missing values was 0.999. Significantly dysregulated proteins were defined as those which had a fold change value > 2 or < −2, with an adjusted p-value of < 0.05.

Immunofluorescent staining

A549 cells: A549 cells in 6-well plates (90% confluence) were transfected with pDZ-IAV NP for 24 hours following the transfection procedures as described above. A549 cells were

incubated with the indicated compounds (working concentrations = 1 μM, 0.1% DMSO) at 37 °C for 8 hours. A549 cells were then washed by PBS, fixed by 4% paraformaldehyde at room temperature for 15 minutes, and immunoblotted by anti-H1N1 NP at 4 °C overnight and anti-rabbit IgG (Alexa Fluor™ Plus 488) at room temperature for 1 hour. A549 cells were washed by PBS after each step of fixation and immunoblotting. DAPI counterstaining was then performed by incubating A549 cells with DAPI in PBS (3 μg/mL) in the dark at room temperature for 15 minutes. A549 cells were finally washed by PBS. Fluorescence images were recorded by EVOS Cell Imaging Systems.

Lung organoids: Lung organoids were infected by WT PR8 virus or SARS-CoV-2 and treated with the indicated compounds following the infection procedures as described above. Lung organoids were fixed in 4% paraformaldehyde in PBS at room temperature for 30 minutes.

For WT PR8 infected organoids, permeabilization and blocking was performed by incubating whole organoids in permeabilization/blocking buffer (5% FBS and 1% TritonX-100 in PBS) with agitation at room temperature for 2 hours. Organoids were washed by immunofluorescence (IF) buffer (0.1% w/v BSA, 0.2% v/v Triton X-100, and 0.1% v/v Tween-20 in PBS). Thereafter, primary antibody staining and secondary antibody staining were processed by incubating organoids in IF buffer containing anti-H1N1 NP (0.5 μg/mL) and anti-rabbit IgG (Alexa Fluor™ Plus 488) (0.5 μg/mL) with agitation at 4 °C overnight, respectively. Organoids were washed by cold IF buffer after each step of staining. DAPI counterstaining was then performed by incubating organoids in IF buffer containing DAPI (3 μg/mL) with agitation in the dark at room temperature for 15 minutes. Organoids were finally washed by water and PBS, respectively. To optically clear the organoids, organoids were incubated in 50% and 100% methanol with agitation in the dark at room temperature for 1 hour, respectively. Methanol was then removed. Organoids were suspended in Vectashield PLUS Antifade Mounting Medium and transferred to μ-Slide 8 well^{high} IbiTreat chamber slides. Stained organoids were then imaged on the Leica SP5 DMI confocal microscope. Images were processed using FIJI.[56]

For SARS-CoV-2 infected organoids, fixed organoids were washed by PBS. Organoids were then immersed in 10% sucrose solution overnight, in 20% sucrose solution overnight, in 30% sucrose solution overnight, and finally in a 1:1 mix of 30% sucrose:OCT solution overnight. Organoids were then embedded in OCT compound and sectioned with a cryostat (Leica) at 7 μm thickness. For immunostaining, sectioned slides were equilibrated to room temperature for 2 hours. Slides were washed in 1x Tris-Buffered Saline for 30min, then permeabilized and blocked using the TrueBlack IF Background Suppressor System (Permeabilizing) (Biotium) following the manufacturer's instructions. Slides were stained by anti-SARS-CoV-2 NP (1:250 dilution) and anti-mouse IgG (Alexa Fluor™ Plus 488) (1:500 dilution) at 4°C overnight, counterstained with DAPI in the dark at room temperature for 15 minutes, and finally mounted. Samples were imaged on the Leica SP5 confocal microscope, and images were processed with FIJI.

Section II RNA destroyers

Synthesis of RNA oligonucleotides: Four biotinylated RNA oligonucleotides (Biotin-RNA 1–4) were directly purchased from Integrated DNA Technologies. RNA oligonucleotides were synthesized by using standard RNA bases, modified by phosphorylation (code: /5Phos/), and conjugated with biotin (code: /5Biosg/and /3Bio/). Destroyer RNA3-A and RNA4-A were customized by Horizon Discovery. RNA oligonucleotides were synthesized by using phosphorothioated 2'-O-methyl RNA bases and conjugated with (S, R, S)-AHPC-PEG6 (BP-25703, BroadPharm) through 5-LC-N-U (code: 5-LC-N-U). The synthesized RNA3-A and RNA4-A were then purified by HPLC.

IAV UTR analysis: Sequences for UTR analysis of IAV were downloaded from the NCBI Influenza Virus Sequence Database and Access and Download date was June 20, 2022.[63] A custom R script was used for analysis. Briefly, full length sequences that had were deemed complete ("c" in column 11 in influenza_na.dat metadata table) were used. As preliminary scans of sequences revealed that many sequences in this first filter bore truncated 3' and 5' UTRs, a further secondary filter was applied. Unique, full length mRNA sequences that started with "AGC" and end with "ACT" nucleotides, were used for downstream analysis. UTR sequences were then demarcated using ORFik Bioconductor package (Release 1.16.0) and then aligned using the DECIPHER Bioconductor package (release 2.24.0).[64,65] To avoid potential biases due to sampling and sequencing errors, only unique UTR sequences that did not vary from the median UTR length by more than 5% were used for multiple sequence alignment (MSA). MSA outputs were then visualized using ggseqlogo.[66] For host and strain breakdown, unique UTR sequences were mapped back to their originating mRNA sequence, and a summary of all associated hosts and strains visualized with pie charts.

Pull-down assay

vPOL co-immunoprecipitation assay: A549 cells in 6-well plates (90% confluence) were infected by WT PR8 virus (MOI = 3) following the infection procedures as described above. 24 hours post infection, cell pellets were collected, washed by PBS, and suspended in 1 mL lysis buffer (150 mM NaCl, 50 mM TrisHCl pH =7.5, 1 mM EDTA, 0.5% NP40, 1× protease and phosphatase inhibitor) in 5 mL tubes. 50 μL 5M NaCl were added into the tubes and cells were lysed by rotating the tubes at 4 °C for 30 minutes. 1 mL H_2O were added into the tubes. The tubes were rotated at 4 °C for 10 minutes and centrifuged at 15,000 rpm for 10 minutes. The supernatants of the cell lysates were then collected for the pull-down assay.

Pull-down assay was processed according to the manufacturer's instructions of Magnetic RNA-Protein Pull-Down Kit. Briefly, the pre-washed and RNase-inactivated streptavidin magnetic beads were coated with Biotin-RNAs in RNA capture buffer (20mM Tris pH 7.5, 1M NaCl, 1mM EDTA) by shaking the beads at 1,000 rpm at 23 °C for 30 minutes. RNA-coated beads were washed by washing buffer (20 mM Tris pH 7.5) and incubated with the supernatants of the cell lysates in protein-RNA binding buffer (20 mM Tris pH 7.5, 50 mM NaCl, 2 mM $MgCl_2$, 0.1% Tween-20, 0.15% glycerol, 0.5U/uL RNase Inhibitor) by shaking the beads at 1,000 rpm at 4 °C for 1 hour. The beads were then washed by washing

buffer (20mM Tris pH 7.5, 10mM NaCl, 0.1% Tween-20). The beads were boiled in 2x Laemmli sample buffer. The eluted samples were collected for processing Western Blots.

VHL co-immunoprecipitation assay: A549 cells in 6-well plates (90% confluence) were infected by FLAG-PB1 PR8 virus (MOI = 3) following the infection procedures as described above. A549 cells were lysed following the same procedures as described in vPOL co-immunoprecipitation assay. The supernatants of the cell lysates were then collected for the pull-down assay.

Pull-down assay was processed according to the manufacturer's instructions of Anti-FLAG M2 Magnetic Beads. Briefly, the pre-washed Anti-FLAG M2 Magnetic Beads were incubated with the supernatants of the cell lysates with or without 1 μM RNA3-A or RNA4-A by gently shaking at 4 °C overnight. The beads were then washed by washing buffer I (150 mM NaCl, 50 mM TrisHCl pH =7.5, 1 mM EDTA) and washing buffer II (150 mM NaCl, 50 mM TrisHCl pH =7.5, 1 mM EDTA, 0.05% NP40). The beads were boiled in 2x Laemmli sample buffer. The eluted samples were collected for processing Western Blots.

RT-PCR

HEK293 cells in 6-well plates (90% confluence) were transfected with 1 μM RNA3-A or RNA4-A for 24 hours following the transfection procedures as described above. Total RNAs were extracted from the cell pellets by using TRIzol Reagent and converted to cDNA by using High-Capacity cDNA Reverse Transcription Kit. RT-PCR was processed by using iQ SYBR Green Supermix.

Flow cytometry—HEK293T cells were seeded in 48-well plates (40% confluence). Wells were coated with 0.5% Gelatin in water at room temperature for 30 minutes prior to plating cells. On the day of flow cytometry, cell culture medium was removed. HEK293T cells were washed by opti-MEM and incubated with NS1-GFP PR8 virus diluted in opti-MEM (MOI = 1) at 37 °C for 1 hour. HEK293T cells were then transfected with 100 μM stocks of the indicated Destroyers (working concentrations = 1 μM) using Lipofectamine RNAiMAX Transfection Reagent according to the manufacturer's instructions. Where indicated, HEK293T cells were also treated with DMSO or 100 nM MG132. 20 hours post infection, cell culture supernatants were collected. HEK293T cell pellets were treated with 0.05% Trypsin-EDTA for at room temperature 3 minutes to achieve single cell suspensions. Trypsinization reactions were stopped by the addition of washing buffer (4% FBS in PBS). HEK293T cells were washed by washing buffer and then passed through 40 μm filters to get single cell suspensions. Flow cytometry experiments were performed on the BD Canto II. Analysis was performed with FCS Express 7 software.

QUANTIFICATION AND STATISTICAL ANALYSIS

Calculations were performed using Graphpad Prism 9. Graphic data in this study are presented as Mean ± SD, n = 2–4. Statistical tests used and significance calculations were performed and shown in each figure legend. Proteomic assays were analyzed as indicated in the method details above.

Supplementary Material

Refer to Web version on PubMed Central for supplementary material.

ACKNOWLEDGEMENTS

I.M. was supported by the Burroughs Wellcome Fund (United States; 1017892), the Chan Zuckerberg Initiative (United States; 2018–191895), the Hirschl Trust Young Investigator fellowship, the NIH U01 0255-E051, and R01 0255-B641. J.J. (Jian Jin) was supported by the NIH SIG grants 1S10OD025132 and 1S10OD028504. Y.C. was supported by the NIH 1R01HL159712–01A1 and W81XWH-21–1-0070. J.S.H was supported by the Charles. H. Revson Senior Fellowship in Biomedical Science.

REFERENCES

1. Morens DM, and Fauci AS (2020). Emerging Pandemic Diseases: How We Got to COVID-19. Cell 182, 1077–1092. 10.1016/j.cell.2020.08.021. [PubMed: 32846157]
2. Taubenberger JK, and Morens DM (2008). The pathology of influenza virus infections. Annu Rev Pathol 3, 499–522. 10.1146/annurev.pathmechdis.3.121806.154316. [PubMed: 18039138]
3. Ho JSY, Zhu Z, and Marazzi I (2021). Unconventional viral gene expression mechanisms as therapeutic targets. Nature 593, 362–371. 10.1038/s41586-021-03511-5. [PubMed: 34012080]
4. Alabi SB, and Crews CM (2021). Major advances in targeted protein degradation: PROTACs, LYTACs, and MADTACs. J Biol Chem 296, 100647. 10.1016/j.jbc.2021.100647. [PubMed: 33839157]
5. Bekes M, Langley DR, and Crews CM (2022). PROTAC targeted protein degraders: the past is prologue. Nat Rev Drug Discov 21, 181–200. 10.1038/s41573-021-00371-6. [PubMed: 35042991]
6. Sakamoto KM, Kim KB, Kumagai A, Mercurio F, Crews CM, and Deshaies RJ (2001). Protacs: chimeric molecules that target proteins to the Skp1-Cullin-F box complex for ubiquitination and degradation. Proc Natl Acad Sci U S A 98, 8554–8559. 10.1073/pnas.141230798. [PubMed: 11438690]
7. Dale B, Cheng M, Park KS, Kaniskan HU, Xiong Y, and Jin J (2021). Advancing targeted protein degradation for cancer therapy. Nat Rev Cancer 21, 638–654. 10.1038/s41568-021-00365-x. [PubMed: 34131295]
8. Desantis J, and Goracci L (2022). Proteolysis targeting chimeras in antiviral research. Future Med Chem 14, 459–462. 10.4155/fmc-2022-0005. [PubMed: 35134309]
9. Li H, Wang S, Ma W, Cheng B, Yi Y, Ma X, Xiao S, Zhang L, and Zhou D (2022). Discovery of Pentacyclic Triterpenoid PROTACs as a Class of Effective Hemagglutinin Protein Degraders. J Med Chem 65, 7154–7169. 10.1021/acs.jmedchem.1c02013. [PubMed: 35579113]
10. Montrose K, and Krissansen GW (2014). Design of a PROTAC that antagonizes and destroys the cancer-forming X-protein of the hepatitis B virus. Biochem Biophys Res Commun 453, 735–740. 10.1016/j.bbrc.2014.10.006. [PubMed: 25305486]
11. de Wispelaere M, Du G, Donovan KA, Zhang T, Eleuteri NA, Yuan JC, Kalabathula J, Nowak RP, Fischer ES, Gray NS, and Yang PL (2019). Small molecule degraders of the hepatitis C virus protease reduce susceptibility to resistance mutations. Nat Commun 10, 3468. 10.1038/s41467-019-11429-w. [PubMed: 31371704]
12. Hahn F, Hamilton ST, Wangen C, Wild M, Kicuntod J, Bruckner N, Follett JEL, Herrmann L, Kheimar A, Kaufer BB, et al. (2021). Development of a PROTAC-Based Targeting Strategy Provides a Mechanistically Unique Mode of Anti-Cytomegalovirus Activity. Int J Mol Sci 22. 10.3390/ijms222312858.
13. Xu Z, Liu X, Ma X, Zou W, Chen Q, Chen F, Deng X, Liang J, Dong C, Lan K, et al. (2022). Discovery of oseltamivir-based novel PROTACs as degraders targeting neuraminidase to combat H1N1 influenza virus. Cell Insight 1, 100030. 10.1016/j.cellin.2022.100030. [PubMed: 37193052]
14. Shaheer M, Singh R, and Sobhia ME (2022). Protein degradation: a novel computational approach to design protein degrader probes for main protease of SARS-CoV-2. J Biomol Struct Dyn 40, 10905–10917. 10.1080/07391102.2021.1953601. [PubMed: 34328382]

15. Zhao J, Wang J, Pang X, Liu Z, Li Q, Yi D, Zhang Y, Fang X, Zhang T, Zhou R, et al. (2022). An anti-influenza A virus microbial metabolite acts by degrading viral endonuclease PA. Nat Commun 13, 2079. 10.1038/s41467-022-29690-x. [PubMed: 35440123]
16. Kao RY, Yang D, Lau LS, Tsui WH, Hu L, Dai J, Chan MP, Chan CM, Wang P, Zheng BJ, et al. (2010). Identification of influenza A nucleoprotein as an antiviral target. Nat Biotechnol 28, 600–605. 10.1038/nbt.1638. [PubMed: 20512121]
17. Manicassamy B, Manicassamy S, Belicha-Villanueva A, Pisanelli G, Pulendran B, and Garcia-Sastre A (2010). Analysis of in vivo dynamics of influenza virus infection in mice using a GFP reporter virus. Proc Natl Acad Sci U S A 107, 11531–11536. 10.1073/pnas.0914994107. [PubMed: 20534532]
18. Zhouravleva G, Frolova L, Le Goff X, Le Guellec R, Inge-Vechtomov S, Kisselev L, and Philippe M (1995). Termination of translation in eukaryotes is governed by two interacting polypeptide chain release factors, eRF1 and eRF3. EMBO J 14, 4065–4072. 10.1002/j.1460-2075.1995.tb00078.x. [PubMed: 7664746]
19. Matyskiela ME, Lu G, Ito T, Pagarigan B, Lu CC, Miller K, Fang W, Wang NY, Nguyen D, Houston J, et al. (2016). A novel cereblon modulator recruits GSPT1 to the CRL4(CRBN) ubiquitin ligase. Nature 535, 252–257. 10.1038/nature18611. [PubMed: 27338790]
20. Sellar RS, Sperling AS, Slabicki M, Gasser JA, McConkey ME, Donovan KA, Mageed N, Adams DN, Zou C, Miller PG, et al. (2022). Degradation of GSPT1 causes TP53-independent cell death in leukemia while sparing normal hematopoietic stem cells. J Clin Invest 132. 10.1172/JCI153514.
21. Jiang L, Zang D, Yi S, Li X, Yang C, Dong X, Zhao C, Lan X, Chen X, Liu S, et al. (2016). A microRNA-mediated decrease in eukaryotic initiation factor 2alpha promotes cell survival during PS-341 treatment. Sci Rep 6, 21565. 10.1038/srep21565. [PubMed: 26898246]
22. Zhu H, Shi X, Ju D, Huang H, Wei W, and Dong X (2014). Anti-inflammatory effect of thalidomide on H1N1 influenza virus-induced pulmonary injury in mice. Inflammation 37, 2091–2098. 10.1007/s10753-014-9943-9. [PubMed: 24912813]
23. Le-Trilling VT, Megger DA, Katschinski B, Landsberg CD, Ruckborn MU, Tao S, Krawczyk A, Bayer W, Drexler I, Tenbusch M, et al. (2016). Broad and potent antiviral activity of the NAE inhibitor MLN4924. Sci Rep 6, 19977. 10.1038/srep19977. [PubMed: 26829401]
24. Widjaja I, de Vries E, Tscherne DM, Garcia-Sastre A, Rottier PJ, and de Haan CA (2010). Inhibition of the ubiquitin-proteasome system affects influenza A virus infection at a postfusion step. J Virol 84, 9625–9631. 10.1128/JVI.01048-10. [PubMed: 20631148]
25. Heaton NS, Moshkina N, Fenouil R, Gardner TJ, Aguirre S, Shah PS, Zhao N, Manganaro L, Hultquist JF, Noel J, et al. (2016). Targeting Viral Proteostasis Limits Influenza Virus, HIV, and Dengue Virus Infection. Immunity 44, 46–58. 10.1016/j.immuni.2015.12.017. [PubMed: 26789921]
26. Chen YW, Huang SX, de Carvalho A, Ho SH, Islam MN, Volpi S, Notarangelo LD, Ciancanelli M, Casanova JL, Bhattacharya J, et al. (2017). A three-dimensional model of human lung development and disease from pluripotent stem cells. Nat Cell Biol 19, 542–549. 10.1038/ncb3510. [PubMed: 28436965]
27. Boye E, and Grallert B (2020). eIF2alpha phosphorylation and the regulation of translation. Curr Genet 66, 293–297. 10.1007/s00294-019-01026-1. [PubMed: 31485739]
28. Hoffmann M, Kleine-Weber H, Schroeder S, Kruger N, Herrler T, Erichsen S, Schiergens TS, Herrler G, Wu NH, Nitsche A, et al. (2020). SARS-CoV-2 Cell Entry Depends on ACE2 and TMPRSS2 and Is Blocked by a Clinically Proven Protease Inhibitor. Cell 181, 271–280 e278. 10.1016/j.cell.2020.02.052. [PubMed: 32142651]
29. Parsons AJ, Cohen T, Schwarz TM, Stein KR, Ophir SI, Casado JP, and Tortorella D (2021). Valspodar limits human cytomegalovirus infection and dissemination. Antiviral Res 193, 105124. 10.1016/j.antiviral.2021.105124. [PubMed: 34197862]
30. Furuse Y, and Oshitani H (2011). Evolution of the influenza A virus untranslated regions. Infect Genet Evol 11, 1150–1154. 10.1016/j.meegid.2011.04.006. [PubMed: 21515407]
31. Ho JSY, Angel M, Ma Y, Sloan E, Wang G, Martinez-Romero C, Alenquer M, Roudko V, Chung L, Zheng S, et al. (2020). Hybrid Gene Origination Creates Human-Virus Chimeric Proteins during Infection. Cell 181, 1502–1517 e1523. 10.1016/j.cell.2020.05.035. [PubMed: 32559462]

32. Pflug A, Guilligay D, Reich S, and Cusack S (2014). Structure of influenza A polymerase bound to the viral RNA promoter. Nature 516, 355–360. 10.1038/nature14008. [PubMed: 25409142]
33. Ayllon J, and Garcia-Sastre A (2015). The NS1 protein: a multitasking virulence factor. Curr Top Microbiol Immunol 386, 73–107. 10.1007/82_2014_400. [PubMed: 25007846]
34. Ochoa S, and Milam VT (2020). Modified Nucleic Acids: Expanding the Capabilities of Functional Oligonucleotides. Molecules 25. 10.3390/molecules25204659.
35. Behlke MA (2008). Chemical modification of siRNAs for in vivo use. Oligonucleotides 18, 305–319. 10.1089/oli.2008.0164. [PubMed: 19025401]
36. Roers A, Hiller B, and Hornung V (2016). Recognition of Endogenous Nucleic Acids by the Innate Immune System. Immunity 44, 739–754. 10.1016/j.immuni.2016.04.002. [PubMed: 27096317]
37. Walsh D, and Mohr I (2011). Viral subversion of the host protein synthesis machinery. Nat Rev Microbiol 9, 860–875. 10.1038/nrmicro2655. [PubMed: 22002165]
38. Hoshino S, Miyazawa H, Enomoto T, Hanaoka F, Kikuchi Y, Kikuchi A, and Ui M (1989). A human homologue of the yeast GST1 gene codes for a GTP-binding protein and is expressed in a proliferation-dependent manner in mammalian cells. EMBO J 8, 3807–3814. 10.1002/j.1460-2075.1989.tb08558.x. [PubMed: 2511002]
39. Surka C, Jin L, Mbong N, Lu CC, Jang IS, Rychak E, Mendy D, Clayton T, Tindall E, Hsu C, et al. (2021). CC-90009, a novel cereblon E3 ligase modulator, targets acute myeloid leukemia blasts and leukemia stem cells. Blood 137, 661–677. 10.1182/blood.2020008676. [PubMed: 33197925]
40. Hansen JD, Correa M, Alexander M, Nagy M, Huang D, Sapienza J, Lu G, LeBrun LA, Cathers BE, Zhang W, et al. (2021). CC-90009: A Cereblon E3 Ligase Modulating Drug That Promotes Selective Degradation of GSPT1 for the Treatment of Acute Myeloid Leukemia. J Med Chem 64, 1835–1843. 10.1021/acs.jmedchem.0c01489. [PubMed: 33591756]
41. Fang J, Pietzsch C, Tsaprailis G, Crynen G, Cho KF, Ting AY, Bukreyev A, de la Torre JC, and Saphire EO (2022). Functional interactomes of the Ebola virus polymerase identified by proximity proteomics in the context of viral replication. Cell Rep 38, 110544. 10.1016/j.celrep.2022.110544. [PubMed: 35320713]
42. Fang J, Pietzsch C, Witwit H, Tsaprailis G, Crynen G, Cho KF, Ting AY, Bukreyev A, Saphire EO, and de la Torre JC (2022). Proximity interactome analysis of Lassa polymerase reveals eRF3a/GSPT1 as a druggable target for host-directed antivirals. Proc Natl Acad Sci U S A 119, e2201208119. 10.1073/pnas.2201208119. [PubMed: 35858434]
43. Nobre LV, Nightingale K, Ravenhill BJ, Antrobus R, Soday L, Nichols J, Davies JA, Seirafian S, Wang EC, Davison AJ, et al. (2019). Human cytomegalovirus interactome analysis identifies degradation hubs, domain associations and viral protein functions. Elife 8. 10.7554/eLife.49894.
44. Gordon DE, Jang GM, Bouhaddou M, Xu J, Obernier K, White KM, O'Meara MJ, Rezelj VV, Guo JZ, Swaney DL, et al. (2020). A SARS-CoV-2 protein interaction map reveals targets for drug repurposing. Nature 583, 459–468. 10.1038/s41586-020-2286-9. [PubMed: 32353859]
45. Dalziel M, Crispin M, Scanlan CN, Zitzmann N, and Dwek RA (2014). Emerging principles for the therapeutic exploitation of glycosylation. Science 343, 1235681. 10.1126/science.1235681. [PubMed: 24385630]
46. Noueiry AO, Olivo PD, Slomczynska U, Zhou Y, Buscher B, Geiss B, Engle M, Roth RM, Chung KM, Samuel M, and Diamond MS (2007). Identification of novel small-molecule inhibitors of West Nile virus infection. J Virol 81, 11992–12004. 10.1128/JVI.01358-07. [PubMed: 17715228]
47. Roberts TL, Sweet MJ, Hume DA, and Stacey KJ (2005). Cutting edge: species-specific TLR9-mediated recognition of CpG and non-CpG phosphorothioate-modified oligonucleotides. J Immunol 174, 605–608. 10.4049/jimmunol.174.2.605. [PubMed: 15634876]
48. Krieg AM, Matson S, and Fisher E (1996). Oligodeoxynucleotide modifications determine the magnitude of B cell stimulation by CpG motifs. Antisense Nucleic Acid Drug Dev 6, 133–139. 10.1089/oli.1.1996.6.133. [PubMed: 8843328]
49. Monteith DK, Henry SP, Howard RB, Flournoy S, Levin AA, Bennett CF, and Crooke ST (1997). Immune stimulation--a class effect of phosphorothioate oligodeoxynucleotides in rodents. Anticancer Drug Des 12, 421–432. [PubMed: 9236857]
50. Aleem A, Akbar Samad AB, and Slenker AK (2022). Emerging Variants of SARS-CoV-2 And Novel Therapeutics Against Coronavirus (COVID-19). In StatPearls.

51. Kronke J, Fink EC, Hollenbach PW, MacBeth KJ, Hurst SN, Udeshi ND, Chamberlain PP, Mani DR, Man HW, Gandhi AK, et al. (2015). Lenalidomide induces ubiquitination and degradation of CK1alpha in del(5q) MDS. Nature 523, 183–188. 10.1038/nature14610. [PubMed: 26131937]
52. Gemechu Y, Millrine D, Hashimoto S, Prakash J, Sanchenkova K, Metwally H, Gyanu P, Kang S, and Kishimoto T (2018). Humanized cereblon mice revealed two distinct therapeutic pathways of immunomodulatory drugs. Proc Natl Acad Sci U S A 115, 11802–11807. 10.1073/pnas.1814446115. [PubMed: 30373817]
53. Roberts TC, Langer R, and Wood MJA (2020). Advances in oligonucleotide drug delivery. Nat Rev Drug Discov 19, 673–694. 10.1038/s41573-020-0075-7. [PubMed: 32782413]
54. Ho JSY, Mok BW, Campisi L, Jordan T, Yildiz S, Parameswaran S, Wayman JA, Gaudreault NN, Meekins DA, Indran SV, et al. (2021). TOP1 inhibition therapy protects against SARS-CoV-2-induced lethal inflammation. Cell 184, 2618–2632 e2617. 10.1016/j.cell.2021.03.051. [PubMed: 33836156]
55. Schneider CA, Rasband WS, and Eliceiri KW (2012). NIH Image to ImageJ: 25 years of image analysis. Nat Methods 9, 671–675. 10.1038/nmeth.2089. [PubMed: 22930834]
56. Schindelin J, Arganda-Carreras I, Frise E, Kaynig V, Longair M, Pietzsch T, Preibisch S, Rueden C, Saalfeld S, Schmid B, et al. (2012). Fiji: an open-source platform for biological-image analysis. Nat Methods 9, 676–682. 10.1038/nmeth.2019. [PubMed: 22743772]
57. Choi M, Chang CY, Clough T, Broudy D, Killeen T, MacLean B, and Vitek O (2014). MSstats: an R package for statistical analysis of quantitative mass spectrometry-based proteomic experiments. Bioinformatics 30, 2524–2526. 10.1093/bioinformatics/btu305. [PubMed: 24794931]
58. Schrodinger LLC (2015). The PyMOL Molecular Graphics System, Version 1.8.
59. Gerritz SW, Cianci C, Kim S, Pearce BC, Deminie C, Discotto L, McAuliffe B, Minassian BF, Shi S, Zhu S, et al. (2011). Inhibition of influenza virus replication via small molecules that induce the formation of higher-order nucleoprotein oligomers. Proc Natl Acad Sci U S A 108, 15366–15371. 10.1073/pnas.1107906108. [PubMed: 21896751]
60. Higgins CA, Nilsson-Payant BE, Kurland AP, Adhikary P, Golynker I, Danziger O, Panis M, Rosenberg BR, tenOever B, and Johnson JR (2021). SARS-CoV-2 hijacks p38ß/MAPK11 to promote viral protein translation. bioRxiv, 2021.2008.2020.457146. 10.1101/2021.08.20.457146.
61. Bruderer R, Bernhardt OM, Gandhi T, Xuan Y, Sondermann J, Schmidt M, Gomez-Varela D, and Reiter L (2017). Optimization of Experimental Parameters in Data-Independent Mass Spectrometry Significantly Increases Depth and Reproducibility of Results. Mol Cell Proteomics 16, 2296–2309. 10.1074/mcp.RA117.000314. [PubMed: 29070702]
62. Elias JE, and Gygi SP (2007). Target-decoy search strategy for increased confidence in large-scale protein identifications by mass spectrometry. Nat Methods 4, 207–214. 10.1038/nmeth1019. [PubMed: 17327847]
63. Bao Y, Bolotov P, Dernovoy D, Kiryutin B, Zaslavsky L, Tatusova T, Ostell J, and Lipman D (2008). The influenza virus resource at the National Center for Biotechnology Information. J Virol 82, 596–601. 10.1128/JVI.02005-07. [PubMed: 17942553]
64. Tjeldnes H, Labun K, Torres Cleuren Y, Chyzynska K, Swirski M, and Valen E (2021). ORFik: a comprehensive R toolkit for the analysis of translation. BMC Bioinformatics 22, 336. 10.1186/s12859-021-04254-w. [PubMed: 34147079]
65. Wright ES (2015). DECIPHER: harnessing local sequence context to improve protein multiple sequence alignment. BMC Bioinformatics 16, 322. 10.1186/s12859-015-0749-z. [PubMed: 26445311]
66. Wagih O (2017). ggseqlogo: a versatile R package for drawing sequence logos. Bioinformatics 33, 3645–3647. 10.1093/bioinformatics/btx469. [PubMed: 29036507]

HIGHLIGHTS

- FM-74–103 inhibits IAV, SARS-CoV-2 and CMV infections through GSPT1 degradation.
- GSPT1 degradation is antiviral as it is a crucial host factor for many viruses.
- Destroyers are viral RNA mimics that target viral proteins for degradation.
- Targeting viral polymerase with destroyers is a virus-specific antiviral strategy.

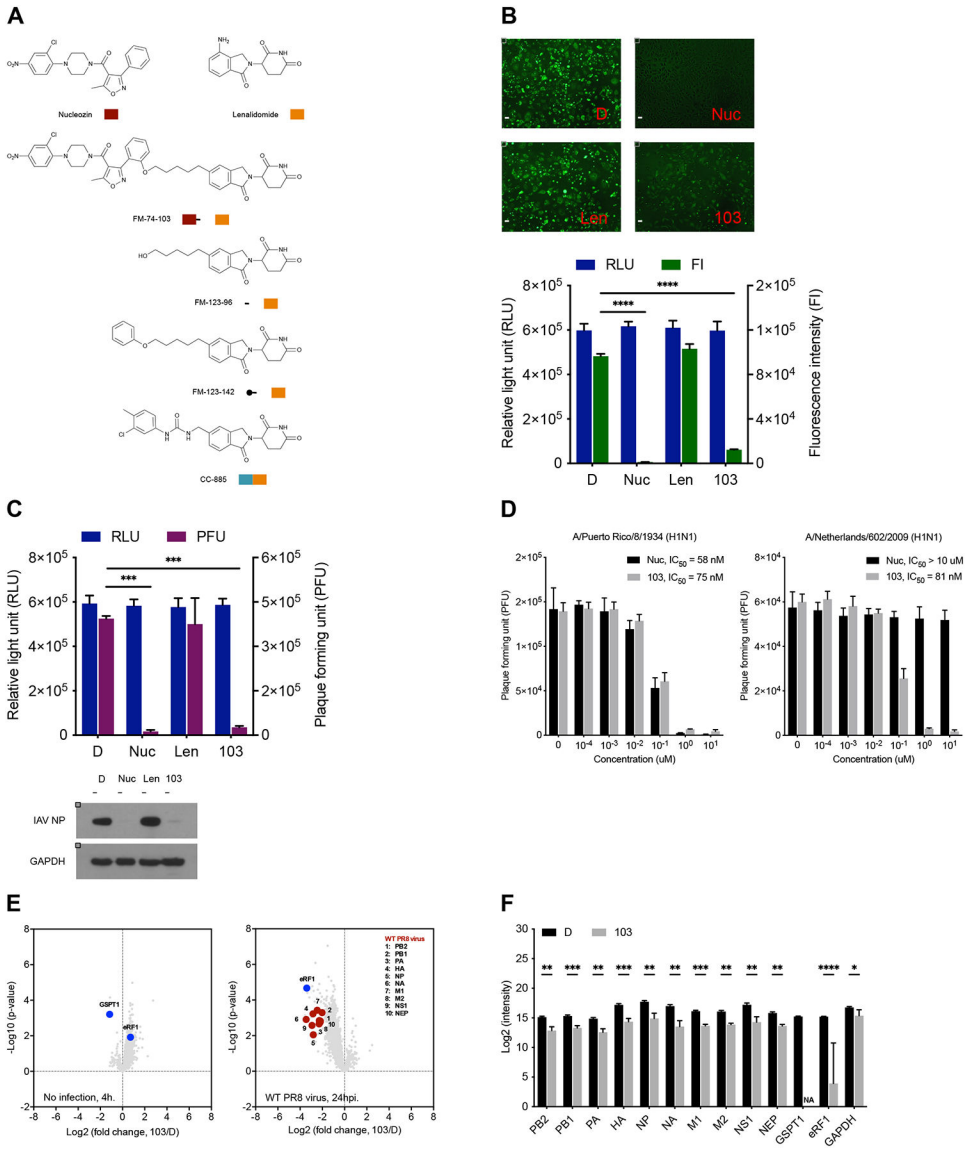

Figures 1. 103 inhibits IAV replication.

A. Structures of the indicated compounds and their cartoon illustrations.

B. (Top) Fluorescence images (scale bars = 400 μm): A549 cells infected by NS1-GFP PR8 virus (MOI = 1) and treated with 1 μM of the indicated compounds for 24 hours post infection. (Bottom) GFP intensities in top panel (green bars and right axis). Mean ± sd, n = 3; CellTiter-Glo luminescence assays: ATP levels in A549 cells treated with 1 μM of the indicated compounds for 24 hours (blue bars and left axis). Mean ± sd, n = 3.

C. (Top) Plaque assays: viral titers in supernatants of A549 cells infected by WT PR8 virus (MOI = 1) and treated with 1 μM of the indicated compounds for 24 hours post infection (purple bars and right axis). Mean ± sd, n = 2; CellTiter-Glo luminescence assays: ATP levels in A549 cells treated with 1 μM of the indicated compounds for 24 hours (blue bars and left axis). Mean ± sd, n = 3. (Bottom) Western blots: A549 cells from the experiments described in top panel.

D. Plaque assays: viral titers in supernatants of HBTE cells infected by A/Puerto Rico/8/34 (H1N1) virus (WT PR8 virus) (MOI=1) (Left) or A/Netherlands/602/2009 (H1N1) virus (MOI=1) (Right) and treated with the indicated concentrations of Nucleozin (black bars) or 103 (grey bars) for 24 hours post infection. IC_{50} are indicated. Mean ± sd, n = 3.

E. Proteomics assay: (Left) Volcano plot of proteomics data from uninfected A549 cells treated with DMSO or 1 μM 103 for 4 hours (No infection, 4h). (Right) Volcano plot of proteomics data from A549 cells infected by WT PR8 virus (MOI = 1) and treated with DMSO or 1 μM 103 for 24 hours post infection (WT PR8 virus, 24hpi). GSPT1/eRF1 and IAV proteins are highlighted in blue and red, respectively. n = 3.

F. Proteomics assay: absolute abundance of the indicated proteins from experiments described in Figure 1E. Mean ± sd, n = 3.

All p-values were calculated by Student's T test. p-value: * < 0.05, ** < 0.01, *** < 0.001, and **** < 0.0001.

D: DMSO, Nuc: Nucleozin, Len: Lenalidomide, NA: Not available.

See also Figure S1.

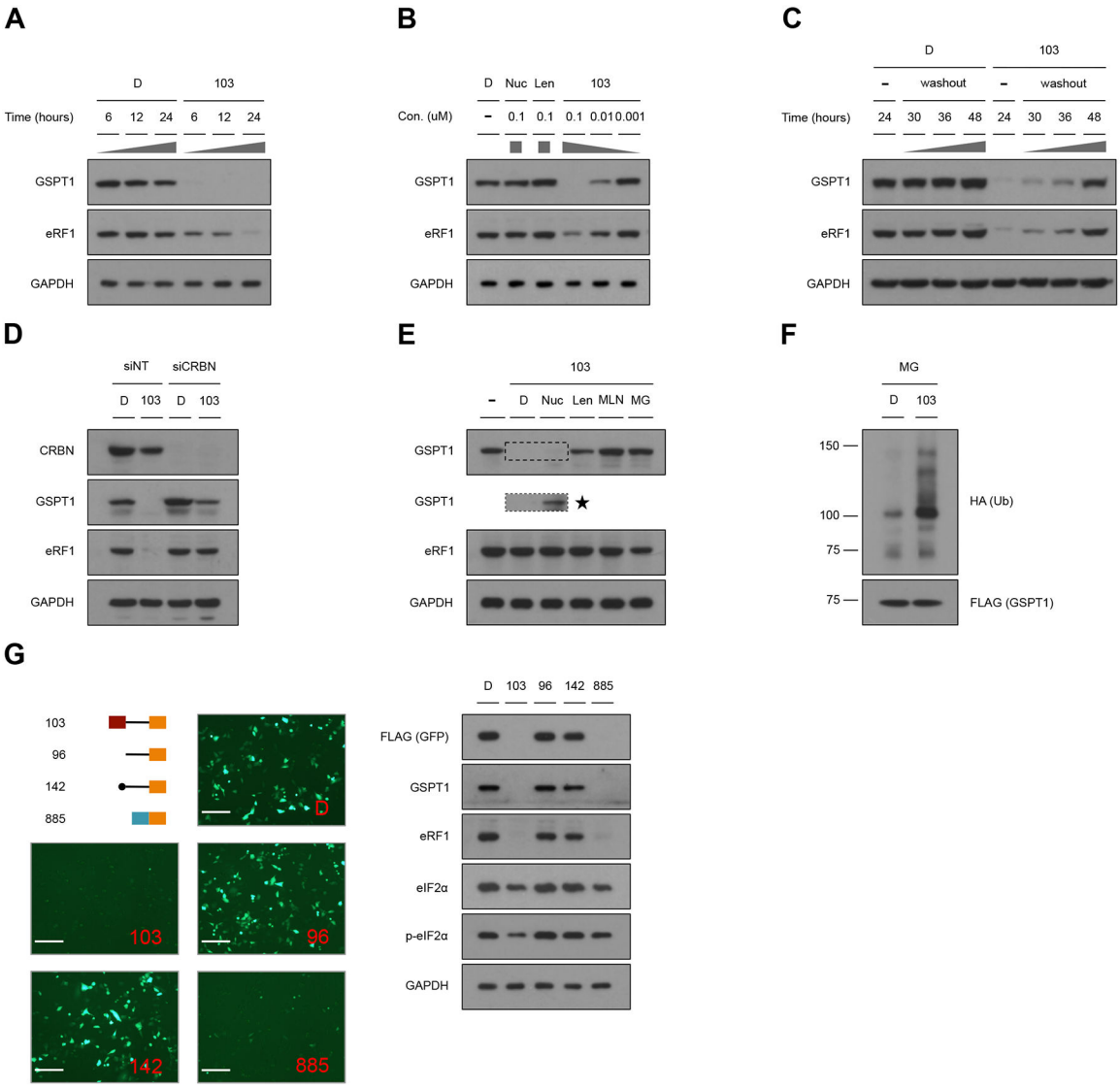

Figures 2. 103 selectively depletes human GSPT1.

A. Western blots: A549 cells treated with DMSO or 0.1 μM 103 for the indicated periods of time.

B. Western blots: A549 cells treated with the indicated compounds at the indicated concentrations for 24 hours.

C. Western blots: A549 cells treated with DMSO or 0.1 μM 103 for 24 hours (−). The medium containing the compounds was then removed and cells were cultured in fresh medium for the indicated periods of time (washout).

D. Western blots: A549 cells transfected with 100 nM non-targeting siRNA (siNT) or siRNA against *CRBN* (siCRBN) for 48 hours, followed by treatment with DMSO or 1 μM 103 for 8 hours.

E. Western blots: A549 cells treated with 10 μM of the indicated competitor compounds for 1 hour, followed by co-treatment with 1 μM 103 for 6 hours. ★: overdeveloped region as defined by the dashed box.

F. Western blots: A549 cells were co-transfected with HA-Ub and FLAG-GSPT1 plasmids for 24 hours, followed by treatment with DMSO or 1 μM 103 for 8 hours. FLAG-GSPT1 with HA-Ub modification was pulled down from cell lysates.

G. Fluorescence images (scale bars = 400 μm) (Left) and western blots (Right): A549 cells were simultaneously transfected with FLAG-GFP plasmid and treated with DMSO or 1 μM of the indicated compounds for 24 hours. Cartoon illustrations are indicated, see also Figure 1A.

D: DMSO, Nuc: Nucleozin, Len: Lenalidomide, MLN: MLN4924, MG: MG-132.

See also Figure S2.

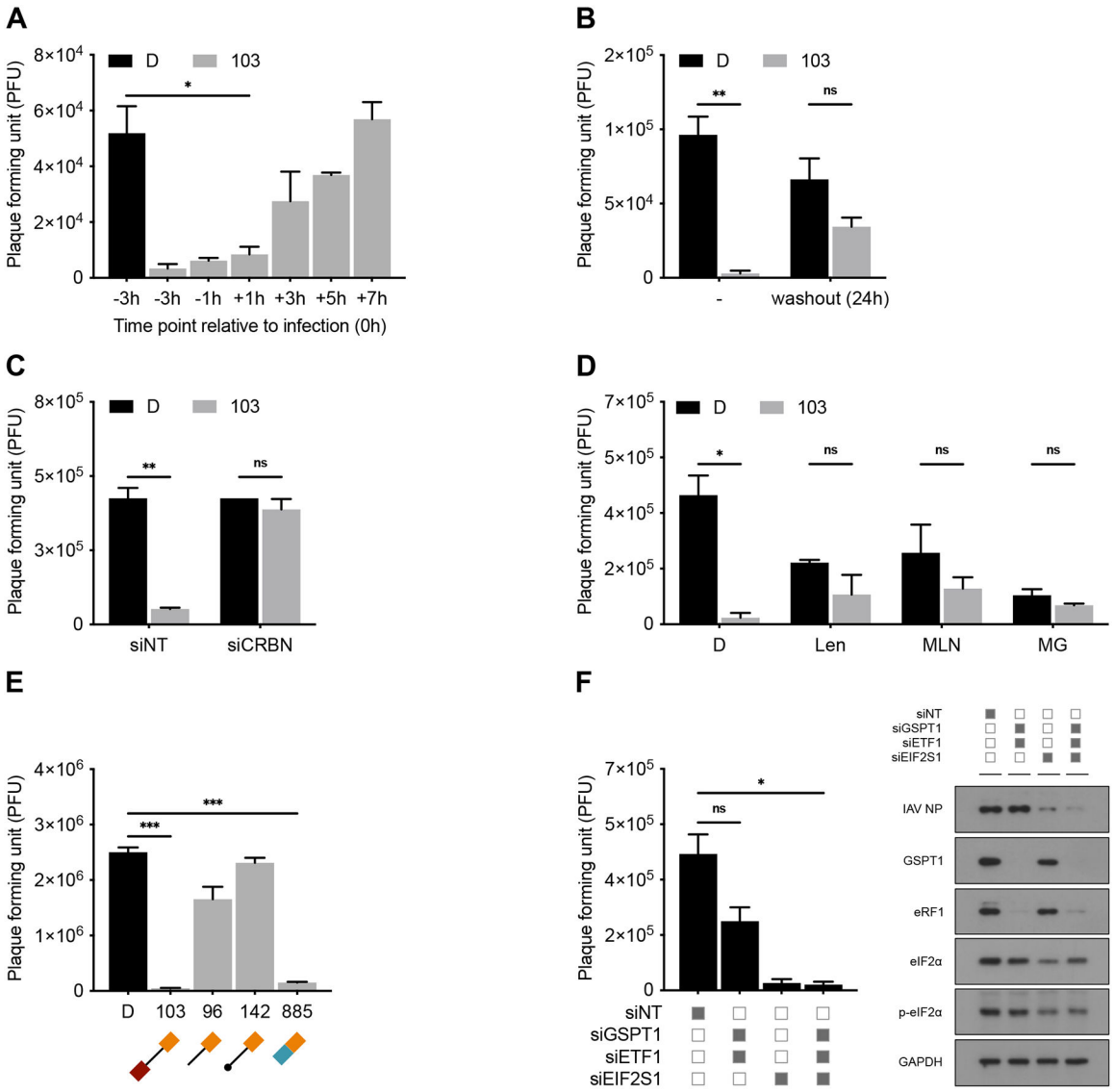

Figures 3. 103-induced degradation of GSPT1 confers anti-IAV effect.

A. Plaque assays: viral titers in supernatants of A549 cells infected by WT PR8 virus (MOI = 1) and treated with DMSO or 1 μM 103 for 24 hours post infection. 103 was added into the medium at the indicated time points before or after infection. Mean ± sd, n = 2.

B. Plaque assays: A549 cells were treated with DMSO or 0.1 μM 103 for 24 hours. The medium containing the compounds were then removed and cells were infected by WT PR8 virus (MOI = 1) and re-treated with DMSO or 1 μM 103 for 24 hours post infection (−) or without re-treatment of the compounds (washout (24h)). Mean ± sd, n = 2.

C. Plaque assays: A549 cells were transfected with 100 nM siNT or siCRBN for 48 hours, followed by being infected by WT PR8 virus (MOI = 1) and treated with DMSO or 1 μM 103 for 3 hours before infection and 24 hours post infection. Mean ± sd, n = 2.

D. Plaque assays: viral titers in supernatants of A549 cells infected by WT PR8 virus (MOI = 1) and treated with DMSO or 1 μM 103 for 3 hours before infection and 24 hours

post infection. Where indicated, A549 cells were concurrently treated with 10 μM of the indicated competitor compounds. Mean ± sd, n = 2.

E. Plaque assays: viral titers in supernatants of A549 cells infected by WT PR8 virus (MOI = 1) and treated with DMSO or 1 μM of the indicated compounds for 3 hours before infection and 24 hours post infection. Cartoon illustrations are indicated, see also Figure 1A. Mean ± sd, n = 2.

F. Plaque assays (Left) and Western blots (Right): A549 cells were transfected with 100 nM siNT, siRNAs against *GSPT1* (siGSPT1), *ETF1* (siETF1), or *EIF2S1* (siEIF2S1) for 72 hours, followed by being infected by WT PR8 virus (MOI = 1) for 24 hours post infection. Mean ± sd, n = 2.

All p-values are calculated by Student's T-test. P-value: ns (not significant) > 0.05, * < 0.05, ** < 0.01, and *** < 0.001.

D: DMSO, Nuc: Nucleozin, Len: Lenalidomide, MLN: MLN4924, MG: MG-132.

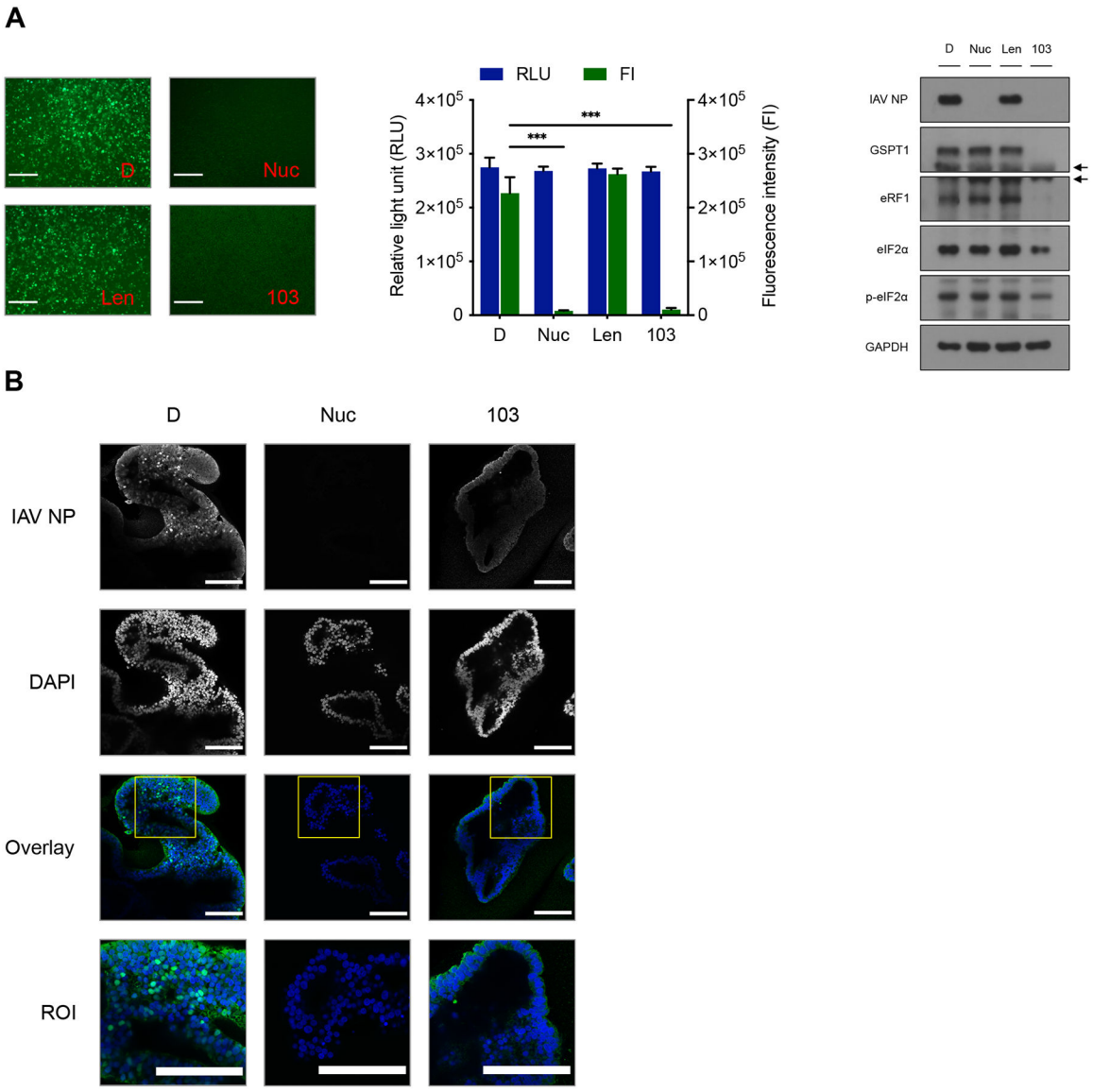

Figures 4. 103 elicits anti-IAV activity in lung organoid model.

A. (Left) Fluorescence images (scale bars = 400 μm): lung organoid-derived epithelial cells infected by NS1-GFP PR8 virus (MOI=1) and treated with DMSO or 1 μM of the indicated compounds for 3 hours before infection and 24 hours post infection. (Middle) GFP intensities of images in left panel (green bars and right axis). Mean ± sd, n = 3; CellTiter-Glo luminescence assays: ATP levels in lung organoid cells treated with 1 μM of the indicated compounds for 24 hours (blue bars and left axis). Mean ± sd, n = 3. All p-values are calculated by Student's T-test. P-value: *** < 0.001. (Right) Western blots: lung organoid cells from the experiments described in left and middle panels. ←: nonspecific bands.

B. Immunofluorescence images (scale bars = 100 μm and 25 μm): 3D lung organoids infected by WT PR8 virus (MOI = 1) and treated with DMSO or 1 μM of the indicated

compounds for 3 hours before infection and 24 hours post infection. Yellow solid boxes: regions of interest (ROI) on overlaying images.
D: DMSO, Nuc: Nucleozin, Len: Lenalidomide.

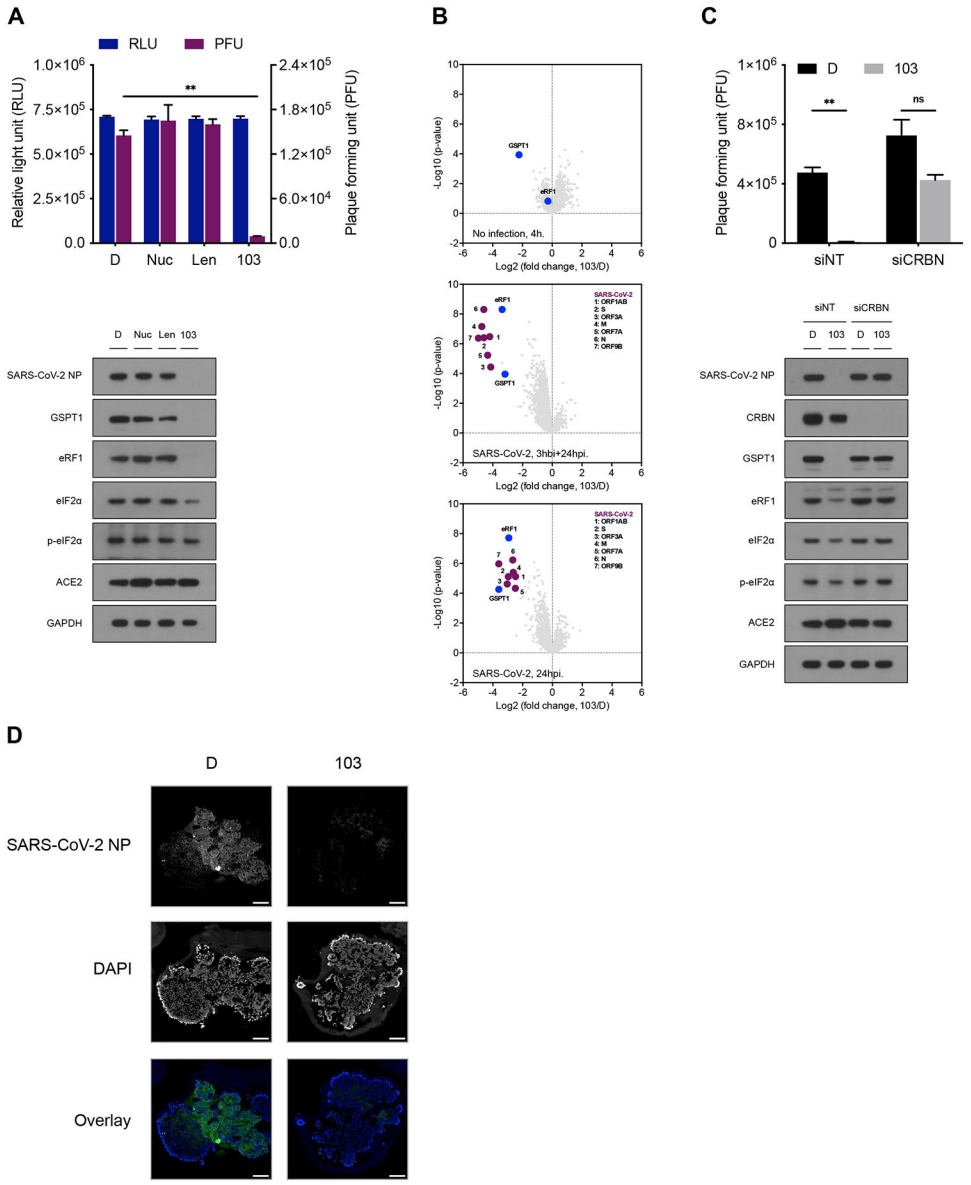

Figures 5. 103 has antiviral activity against SARS-CoV-2.

A. (Top) plaque assays: viral titers in supernatants of A549-ACE2 cells infected by SARS-CoV-2 (MOI = 1) and treated with DMSO or 1 μM of the indicated compounds for 3 hours before infection and 24 hours post infection (purple bars and right axis). Mean ± sd, n = 2; CellTiter-Glo luminescence assays: ATP levels in A549-ACE2 cells treated with 1 μM of the indicated compounds for 24 hours (blue bars and left axis). Mean ± sd, n = 3. (Bottom). Western blots: A549-ACE2 cells from the experiments described in top panel.

B. Proteomics assay: (Top) Volcano plot of proteomics data from uninfected A549-ACE2 cells treated with DMSO or 1 μM 103 for 4 hours (No infection, 4h); (Middle) Volcano plot of proteomics data from A549-ACE2 cells infected by SARS-CoV-2 (MOI = 1) and treated with DMSO or 1 μM 103 for 3 hours before infection and 24 hours post infection (SARS-CoV-2, 3hbi+24hpi); (Bottom) Volcano plot of proteomics data from A549-ACE2 cells infected by SARS-CoV-2 (MOI = 1) and treated with DMSO or 1 μM 103 for 24

hours post infection (SARS-CoV-2, 24hpi). GSPT1/eRF1 and SARS-CoV-2 proteins are highlighted in blue and purple, respectively. n = 3.

C. (Top) Plaque assays: A549-ACE2 cells were transfected with 100 nM siNT or siCRBN for 48 hours, followed by being infected by SARS-CoV-2 (MOI = 1) and treated with DMSO or 1 μM 103 for 3 hours before infection and 24 hours post infection. Mean ± sd, n = 2. (Bottom) Western blots: A549-ACE2 cells from the experiments described in top panel.

D. Immunofluorescence images (scale bars = 100 μm): 3D lung organoids infected by SARS-CoV-2 (MOI = 1) and treated with DMSO or 1 μM 103 for 3 hours before infection and 24 hours post infection.

All p-values were calculated by Student's T test. P-value: ns (not significant) > 0.05, ** < 0.01.

D: DMSO, Nuc: Nucleozin, Len: Lenalidomide.

See also Figure S3.

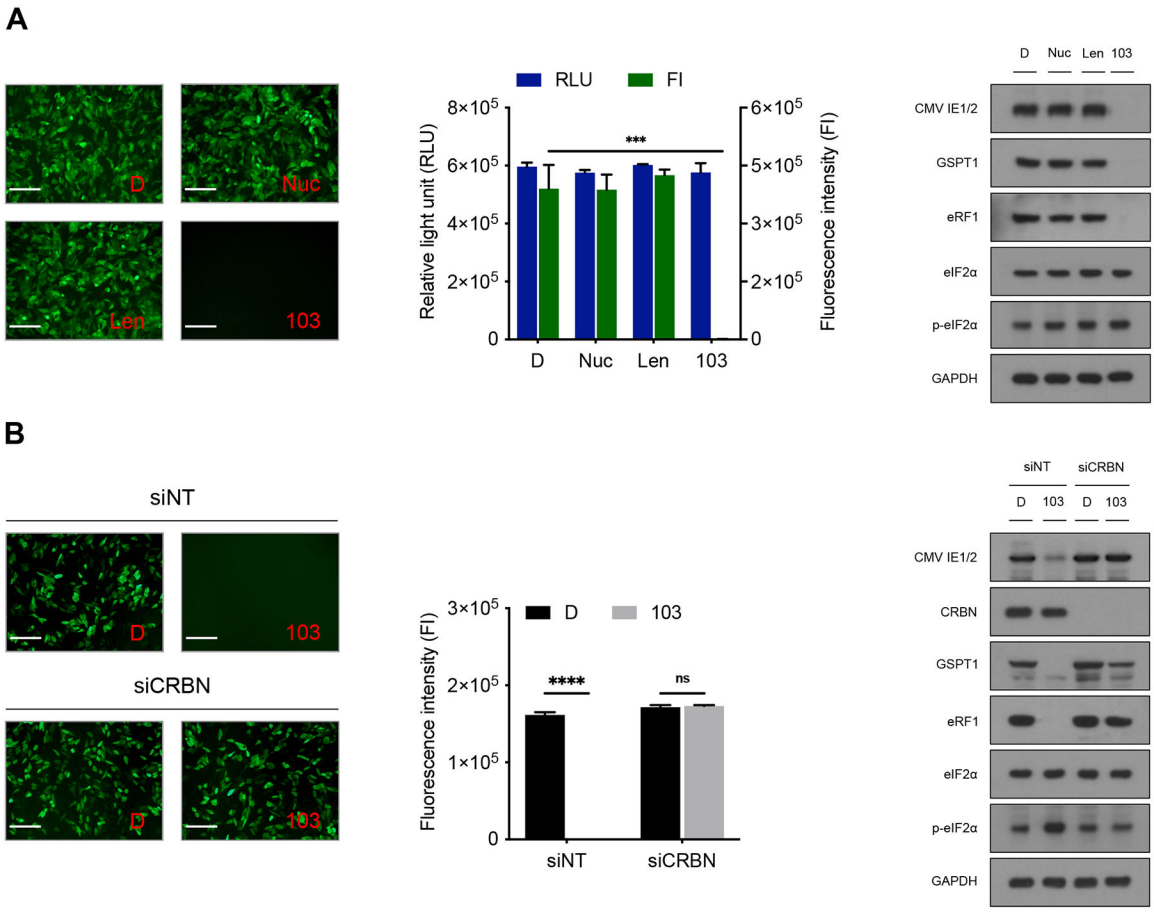

Figures 6. 103 has antiviral activity against CMV.

A. (Left) Fluorescence images (scale bars = 400 μm): ARPE-19 cells infected by AD169^{BADrUL131} virus (MOI = 1) and treated with DMSO or 1 μM of the indicated compounds for 3 hours before infection and 24 hours post infection. (Middle) GFP intensities of images in left panel (green bars and right axis). Mean ± sd, n = 3; CellTiter-Glo luminescence assays: ATP levels in ARPE-19 cells treated with 1 μM of the indicated compounds for 24 hours (blue bars and left axis). Mean ± sd, n = 3. (Right) Western blots: ARPE-19 cells from the experiments described in left and middle panels.

B. (Left) Fluorescence images (scale bars = 400 μm): ARPE-19 cells were transfected with 100 nM siNT or siCRBN for 48 hours, followed by being infected by AD169^{BADrUL131} virus (MOI = 1) and treated with DMSO or 1 μM 103 for 3 hours before infection and 24 hours post infection. (Middle) GFP intensities of images in left panel (green bars and right axis). Mean ± sd, n = 3; CellTiter-Glo luminescence assays: ATP levels in ARPE-19 cells treated with 1 μM of the indicated compounds for 24 hours (blue bars and left axis). Mean ± sd, n = 3. (Right) Western blots: ARPE-19 cells from the experiments described in left and middle panels.

All p-values were calculated by Student's T test. P-value: ns (not significant) > 0.05, *** < 0.001, and **** < 0.0001.

D: DMSO, Nuc: Nucleozin, Len: Lenalidomide.

See also Figure S4.

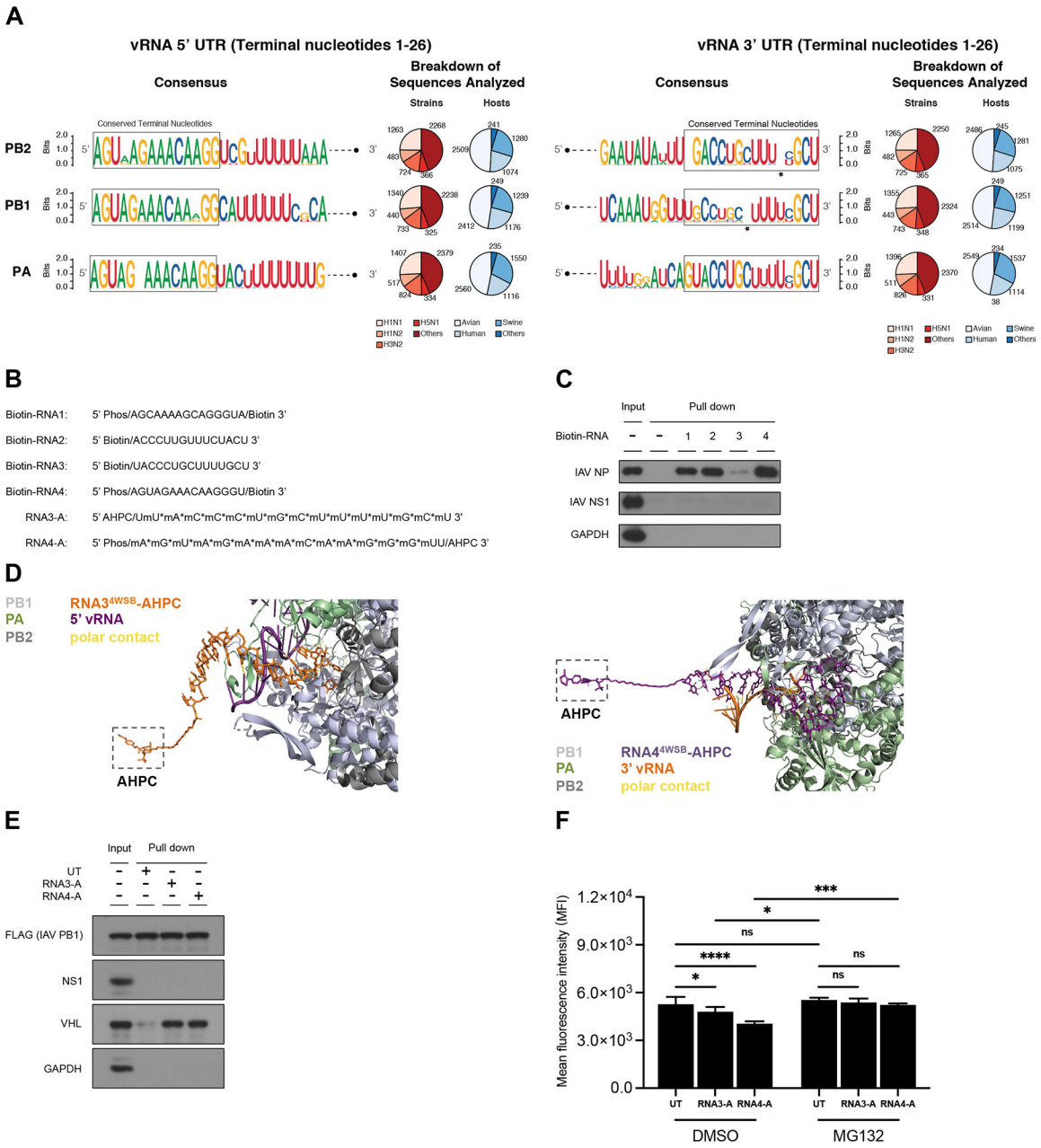

Figures 7. TPD promoted by RNA mimics exhibits anti-IAV activity.a

A. Conserved terminal sequences of IAV segments 1 through 3. Publicly available and unique full-length UTR sequences of the indicated viral segments (vRNA) were aligned. Total number of sequences, the breakdown of contributing strains (H1N1, H1N2, H3N2, H5N1, and others) and host species (Avian, Human, Swine and others) are indicated in the pie charts.

B. Sequences and modifications of Biotin-RNAs and Destroyers. *: phosphorothioate backbones; m: 2'O-methyl modifications; Phos: phosphorylation.

C. Western blots: A549 cells were infected by WT PR8 virus (MOI = 1) for 24 hours. IAV NP was pulled down by 1 μM of the indicated Biotin-RNA oligonucleotides from cell lysates.

D. Visualization of RNA3-A in orange (Left) and RNA4-A in purple (Right) on top of the crystal structure of vPOL and vRNAs (5' vRNA in purple; 3' vRNA in orange) (PDB 4WSB) using Pymol. The original vRNA oligonucleotide sequences used in PDB 4WSB were retained for this analysis. Black dashed boxes: AHPC; Yellow dashed lines: polar contacts.

E. Western blots: A549 cells were infected by FLAG-PB1 PR8 virus (MOI = 1) for 24 hours. IAV PB1 and VHL were pull down by 1 μM RNA3-A or RNA4-A from cell lysates.

F. Flow cytometry: HEK293T cells were infected by NS1-GFP PR8 virus (MOI = 1) and transfected with 1 μM RNA3-A or RNA4-A for 24 hours post infection in the presence or absence of 100 nM MG132. Mean ± sd, n = 3–4. All p-values were calculated by one-way ANOVA followed by Sidak multiple comparisons test. p-value: ns (not significant) > 0.1234, * < 0.0332, **** p < 0.0001. UT: untreated.

See also Figure S5.

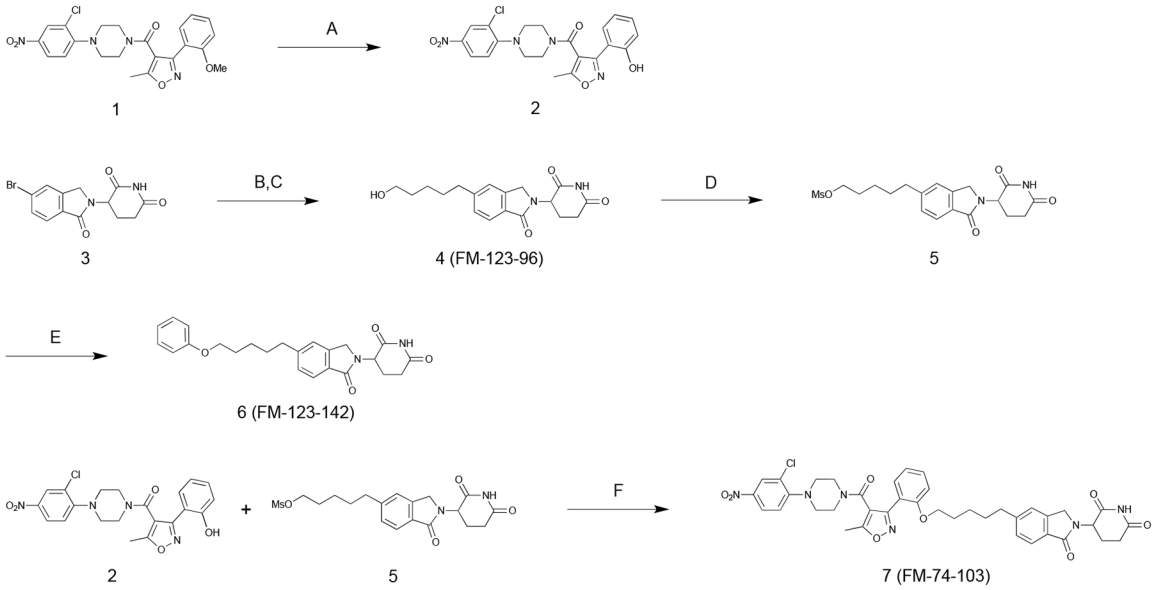

Scheme 1.
Synthetic route of compound FM-123–96, FM-123–142 and FM-74–103

KEY RESOURCES TABLE

REAGENT or RESOURCE	SOURCE	IDENTIFIER
Antibodies		
anti-GSPTI	Cell Signaling Technology	Cat: 14980 RRID: AB_2798677
anti-eRF1	Cell Signaling Technology	Cat: 13916 RRID: AB_2798344
anti-eIF2a	Cell Signaling Technology	Cat: 9722 RRID: AB_2230924
anti-p-eIF2a (Ser51)	Cell Signaling Technology	Cat: 9721 RRID: AB_330951
anti-CRBN	Cell Signaling Technology	Cat: 71810 RRID: AB_2799810
Anti-VHL	Cell Signaling Technology	Cat: 68547 RRID: AB_2716279
anti-ACE2	Abcam	Cat: ab108209 RRID: AB_10862654
anti-GAPDH	Cell Signaling Technology	Cat: 5174 RRID: AB_10622025
anti-H1N1 NP	GenScript	Cat: A01506 RRID: AB_1968881
anti-SARS-CoV-2 NP	Center for Therapeutic Antibody Development at Mount Sinai	Clone 1C7C7
Anti-CMV IE1/2	Abcam	Cat: ab53495 RRID: AB_882995
anti-FLAG M2	Sigma-Aldrich	Cat: A8592 RRID: AB_439702
Anti-HA	Cell Signaling Technology	Cat: 3724 RRID: AB_1549585
anti-rabbit IgG (HRP)	Sigma-Aldrich	Cat: GENA9340 RRID: AB_772191
anti-mouse IgG (HRP)	Sigma-Aldrich	Cat: GENA9310 RRID: AB_772193
anti-rabbit IgG (Alexa Fluor™ Plus 488)	ThermoFisher	Cat: A-11008 RRID: AB_143165
anti-mouse IgG (Alexa Fluor™ Plus 488)	ThermoFisher	Cat: A-11001 AB_2534069
Bacterial and virus strains		
NS1-GFP PR8 virus	Manicassamy *et al.*[17]	N/A
WT PR8 virus	Manicassamy *et al.*[17]	N/A
FLAG-PB1 virus	Heaton *et al.*[25]	N/A
SARS-related coronavirus 2 (SARS-CoV-2), isolate USA-WA1/2020	BEI Resources	NR-52281
AD169BADrUL131 virus	Parsons *et al.*[29]	N/A
Chemicals, peptides, and recombinant proteins		
Nucleozin	Sigma-Aldrich	N2790
MG-132	Sigma-Aldrich	M7449
Lenalidomide	MedChemExpress	HY-A0003
MLN4924	MedChemExpress	HY-70062
CC-885	MedChemExpress	HY-101488
Lipofectamine 3000 Transfection Reagent	ThermoFisher	L3000001
Lipofectamine RNAiMAX Transfection Reagent	ThermoFisher	13778030
TRIzol Reagent	ThermoFisher	15596018
Protease and Phosphatase Inhibitor	ThermoFisher	78444
RNase Inhibitor	ThermoFisher	AM2682
Critical commercial assays		

REAGENT or RESOURCE	SOURCE	IDENTIFIER
CellTiter-Glo Cell Viability Assay	Promega	G7572
MTT Assay Kit	Abcam	ab211091
Western ECL Substrate	Bio-Rad Laboratories	1705061
iQ SYBR Green Supermix	Bio-Rad Laboratories	1708882
TrueBlue Peroxidase Substrate	SeraCare	5510–0030
Anti-FLAG® M2 Magnetic Beads	Sigma-Aldrich	M8823
cDNA Reverse Transcription Kit	ThermoFisher	4368813
Magnetic RNA-Protein Pull-Down Kit	ThermoFisher	20164
Micro BCA™ Protein Assay Kit	ThermoFisher	23235
Deposited data		
Proteomics Data (Figure 1E, 1F, Supplementary Table S1)	This study	PRIDE: PXD042352
Proteomics Data (Figure 5B and S3, Supplementary Table S2)	This study	PRIDE: PXD042352
PDB 4WSB	Pflug *et al.*[32]	N/A
Experimental models: cell lines		
A549	ATCC	Cat: CCL-185 RRID: CVCL_0023
HBTE	ATCC	PCS-300–010
ARPE-19	ATCC	Cat: CRL-2302 RRID: CVCL_0145
MDCK	ATCC	Cat: CCL-34 RRID: CVCL_0422
Vero E6	ATCC	Cat: CRL-1586 RRID: CVCL_0574
HEK293T	ATCC	Cat: CRL-3216 RRID: CVCL_0063
A549-ACE2	Ho et al.[54]	N/A
NHDF	Parsons *et al.*[29]	N/A
Oligonucleotides		
Non-targeting Control siRNA Pool	Horizon Discovery	D-001810–10
Human CRBN siRNA Pool	Horizon Discovery	L-021086–00
Human GSPT1 siRNA Pool	Horizon Discovery	L-019644–00
Human ETF1 siRNA Pool	Horizon Discovery	L-019840–00
Human EIF2S1 siRNA Pool	Horizon Discovery	L-015389–01
Biotin-RNA1–4	This study	N/A
RNA3-A and RNA4-A	This study	N/A
RT-PCR primers	This study	Supplementary Table 3
Recombinant DNA		
pDZ-H1N1 NP	This study	N/A
pcDNA3.1(+)-FLAG-GFP	This study	N/A
pcDNA3.1(+)-FLAG-PSD95	This study	N/A
pcDNA3.1(+)-FLAG-NCBP20	This study	N/A
pcDNA3.1(+)-FLAG-DXO	This study	N/A
pcDNA3.1(+)-FLAG-H1N1 NS1	This study	N/A
pRK5-HA-Ub-WT	Addgene	17608; RRID:Addgene_17608

REAGENT or RESOURCE	SOURCE	IDENTIFIER
pCMV6-Entry-FLAG-GSPT 1	OriGene	RC229318
Software and algorithms		
Graphpad Prism 9	Graphpad	https://www.graphpad.com/
ImageJ	Schneider et al.[55]	https://imagej.net
FIJI	Schindelin et al.[56]	https://imagej.net
MSstats	Choi et al.[57]	N/A
PyMOL version 2.1	Schrödinger.[58]	N/A